DIFFERENTIATING HEALTHY AND BARK BEETLE INFECTED SPRUCE TREES WITH SENTINEL-1 SAR

PHUNTSHO
JULY 2020

SUPERVISORS:
dr. I.C. van Duren
dr. ir. C.A.J.M. de Bie

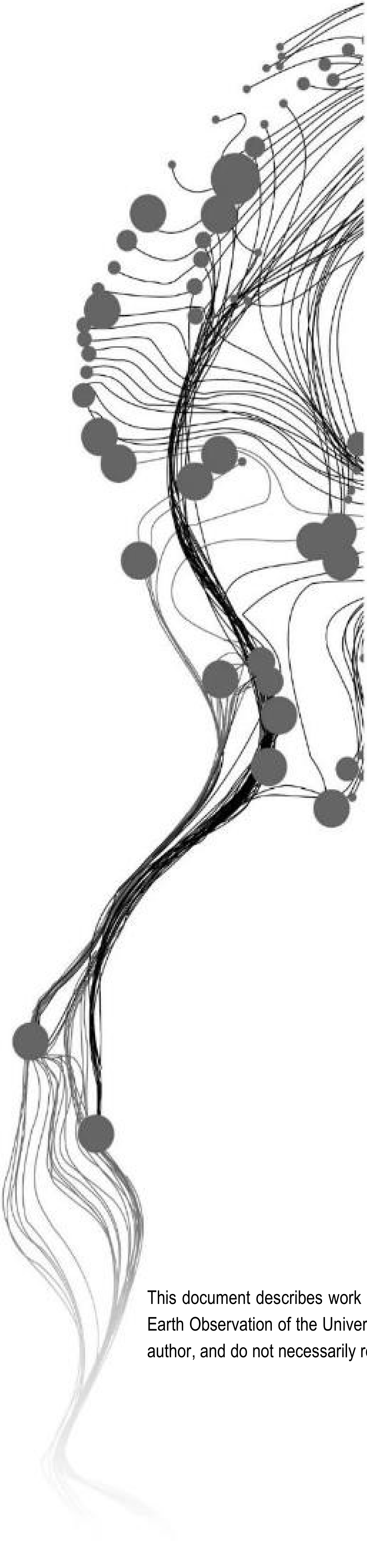

DIFFERENTIATING HEALTHY AND BARK BEETLE INFECTED SPRUCE TREES WITH SENTINEL-1 SAR

PHUNTSHO
Enschede, The Netherlands, JULY 2020

Thesis submitted to the Faculty of Geo-Information Science and Earth Observation of the University of Twente in partial fulfilment of the requirements for the degree of Master of Science in Geo-information Science and Earth Observation.
Specialization: Natural Resource Management

SUPERVISORS:
dr. I.C. van Duren
dr. ir. C.A.J.M. de Bie

THESIS ASSESSMENT BOARD:
dr. L.L.J.M. Willemen (Chair)
dr. ir. W. Bijker (External Examiner, University of Twente)

ABSTRACT

Forests are affected by insect pests globally resulting in tree mortality, and in Europe, the spruce bark beetle (*Ips typographus*) is known to have a large scale detrimental impact on Norway spruce (*Picea abies*) forests. Bark beetle infestations of the spruce trees have significant economic, social, and environmental impacts. The conventional method of field surveying is challenging in terms of resources to identify and differentiate healthy and infected spruce trees. There is a need for a cost-effective remote sensing technology to identify the sites of the bark beetle damaged spruce trees. The ability of remote sensing methods to identify bark beetle infected tree would help mitigate the further spread of the infestation and manage sustainable forest management. The study aims to determine the applicability of the Sentinel-1 SAR data and explore the method to differentiate between the healthy and bark beetle infected spruce trees.

The study was conducted inside the Eifel National Park (ENP) in the North Rhine-Westphalia state of Western Germany. Google Earth imagery was used to obtain the samples for both healthy and infected spruce trees. A single time snapshot of the Sentinel-1 SAR image of the area was analyzed to compare the difference in Sentinel-1 backscatter response between the healthy and infected spruce trees statistically. Sentinel-1 SAR and Sentinel-2 image from 2014 to 2019 were used to extract SAR backscatter and NDRE spectral index, respectively. Temporal profile of healthy and bark beetle infected spruce trees was developed based on the time series of SAR backscatter and the time series of NDRE spectral index. An independent site outside the study area was used to validate the annual pattern of the SAR temporal to ascertain the robustness of the temporal profiling technique.

The distribution of Sentinel-1 SAR backscatter response of a healthy and infected spruce tree overlap substantially, limiting the potential of SAR backscatter to differentiate between them, despite a statistically significant difference with their mean backscatter response. The Sentinel-1 SAR temporal profile of the healthy spruce tree shows an annual seasonal pattern. Adaptive Savitzky-Golay filter (ASAVGOL) helped to produce a pronounced annual profile pattern of the healthy spruce trees. On the other hand, the SAR temporal profile of a bark beetle infected spruce trees shows an irregular temporal profile pattern. The transition from an annual seasonal pattern to an irregular pattern on a temporal profile can be interpreted as the moment of a bark beetle infestation. There was no field data available at each stage of the infestation to relate with the moment of infestation. However, the ability of the temporal profiling method to graphically indicate a point of infestation was verified based on an independent site outside the study area using a discrete set of Sentinel-1 SAR temporal profile analysis.

The temporal profiling method is suitable to exploit the Sentinel-1 SAR to approximately identify the moment of infestation on the time series profile. The moment of infestation shown by the SAR temporal profile is likely related to the annual phenological processes of healthy living trees and bark beetles infected dying trees. Dense weather independent time-series Sentinel-1 images facilitated to graphically visualize an annual pattern on a temporal profile, while the availability of fewer cloud-free Sentinel-2 observations impeded in showing the annual pattern explicitly. Understanding the moment of infestation would facilitate to identify the bark beetle affected sites for forest management applications. It will guide timely sanitation fellings to limit the further spread, though it may not alert forest managers to react immediately as not every deviation from the expected seasonal pattern is pointing at an infestation. Similarly, we can assess whether a timely bark beetle mitigation measures are being implemented or not, and make informed decisions on the sustainable status certification of sustainable forest management. It can be applied by relevant agencies to make an informed decision on the entitlement of the bark beetle damage compensation. Further investigation is necessary to understand at what stage of bark beetle infestation can be described by the SAR temporal profile using field-based samples at each stage of the bark beetle infestation in spruce forests.

ACKNOWLEDGEMENTS

I would like to thank my supervisors Dr. I.C. van Duren (Iris) and Dr. Ir. C.A.J.M. de Bie (Kees) for their valuable guidance and support throughout the research processes.

I would also like to thank Dr. Mohammad Abdel-Razek and the Global Risk Assessment Services GmbH (GRAS) team at Cologne, Germany for the opportunity to work on the satellite images during the internships.

I owe humble gratitude to OKP Scholarship Programme for providing me with an opportunity to peruse this MSc in the Netherlands.

Finally, I want to thank my family and friends for always supporting me.

TABLE OF CONTENTS

LIST OF FIGURES

LIST OF TABLES

LIST OF APPENDIX

LIST OF ACRONYM

ASF	Alaska Satellite Facility
ASAVGOL	Adaptive Savitzky-Golay filter
dB	decibel
ESA	European Space Agency
ENP	Eifel National Park
GIS	Geographical Information System
GFOI	Global Forest Observations Initiative
GPS	Global Positional System
GRAS	Global Risk Assessment Services GmbH
GRD	Ground Range Detected
IPCC	Intergovernmental Panel on Climate Change
KMZ	Keyhole Markup language Zipped
LANDSAT	Land Satellite
NDRE	Normalised Difference Rededge Index
NDVI	Normalized Difference Vegetation Index
QGIS	Quantum GIS
R	Project for Statistical Computing software
SAR	Synthetic Aperture Radar
SLC	Single Look Complex
SNAP	Sentinel Application Platform
SPOT	Satellite Pour l'Observation de la Terre (Satellite for Earth Observation)
TM	Thematic Mapper
VH	Vertical-Transmit and Horizontal-Receive
VV	Vertical-Transmit and Vertical-Receive

1. INTRODUCTION

1.1. Bark beetle infestation of a spruce trees in forests

Forests are affected by insect pests globally, resulting in tree mortality (Wermelinger, 2004). Bark beetle infestations in conifer forests are recorded from the temperate and boreal regions of North America and Central Europe (Scott et al., 1984; Siccama et al., 1982). In Europe, spruce bark beetle (*Ips typographus*) is known to have a large scale detrimental impact on Norway spruce (*Picea abies*) forests (Öhrn et al., 2014). Bark beetles feed on phloem tissues, reproduce inside the bark and infuse phloem-infesting fungi that cause mortality of the host tree due to disruption of the flow of water and nutrients (Solheim, 1992). When bark beetle populations are low, healthy trees defend by producing resin or latex which is called as an endemic phase but after population increases, they overwhelm the defence mechanism of trees which is termed as an epidemic phase or referred to as bark beetle infestations (Boone et al., 2011; Ryan et al., 2015).

Bark beetle infestations are categorized into three different stages, namely as green-attack, red-attack, and grey-attack (Niemann & Visintini, 2005; White et al., 2007). As per those studies, the green attack happens at the initial colonization of the host tree by beetles where no apparent changes appear in the forest canopies. The red attack was reported to occur after one to three years and the foliage of the infected tree turns into a reddish colour. The grey-attack stage was referred to the shedding off needle leaves of the trees. However, the healthy and bark beetle infected spruce trees were the two categories considered for the analysis in this study. Hence, spruce trees are assumed as healthy, when they appear green in the natural colour combination of a satellite image, but after they change their colour from green to reddish or grey, they are considered as bark beetle infected trees. Therefore, identifying bark beetle infestations or differentiating healthy and infected spruce trees refers to the ability to categorize the spruce trees into either healthy or infected trees within a spruce forest area based on this remote sensing study.

1.2. Factors influencing bark beetle infestations in forests

Bark beetle infestation is typically known to be triggered by natural disturbance such as windthrow, storm events, or lightening which causes physical damage of the trees and increases the availability of vulnerable hosts (Cailleret et al., 2014). However, some other studies (Bentz et al., 2019) also suggest that bark beetles usually attack trees already weakened by diseases. Biedermann et al. (2019) point out that intensification of forest management in Europe towards homogeneous spruce stand poses a higher risk for bark beetle infestation. Pureswaran et al., (2018) reported that the changing climate and global warming have increased the susceptibility and risk of bark beetle outbreaks. Many studies claim that weather events such as droughts and the rising temperature are usually followed by bark beetle outbreaks (Kolb et al., 2016; Müller, 2011; Pureswaran et al., 2018). Studies also show that warming climate has enhanced bark beetle reproduction and survival in new regions and higher altitudes (Cailleret et al., 2014; Kautz et al., 2014; Kolb et al., 2016). Considering the current changing climate scenario (IPCC, 2018), identifying and differentiating the bark beetle infected spruce tree is essential to safeguard the widespread damage of the spruce forests.

1.3. Socio-economic impacts of bark beetle infestations of the spruce forests

Bark beetle infestations of trees in the forests have significant economic, social, and environmental impacts (Hlásny et al., 2019; Langstrom et al., 2009). Boyd et al. (2013) studied that forest pests negatively affect ecosystem services due to a change in the structure of the forests such as biodiversity, carbon sink and recreation. In Germany, Müller (2011) looked at how social unrest and political conflict is sparked with bark beetle disturbance of the forests in Bavarian National Park. Similarly, in Slovakia and Czech Republic, social unrest such as public protests and involvement of European Union authorities in forest management issues were all related to beetle infestation (Hlásny et al., 2019). In Germany, from January 2018 to March 2019, about 114,000 hectares of the spruce forest was damaged by bark beetle (Deutsche Welle, 2019). The Ministry of the Environment had to provision more than eight million euros for 2019 and 2020 to aid forest owners in reclaiming and salvaging bark beetle affected forests (Teller Report, 2019). Therefore, there is a growing concern among the forest managers, private forest owners, and forest governance agencies to tackle issues such as lack of efficient tools and information on the incidence of the bark beetle infestations to guide informed decision making (Hlásny et al., 2019; Kolb et al., 2016; Křivan et al., 2016; Pellizzoni, 2011).

1.4. Methods of identifying the bark beetle infestations in a spruce forests

According to Hlásny et al. (2019), the most effective way to reduce beetle devastation of the forest is though sanitation operations which are commonly practised in Europe and worldwide. Sanitation operations refer to finding and eliminating infected spruce trees breaking the chain of the successive beetle reproduction to contain further spreading to healthy trees. Currently, the most common method of identifying bark beetle infestation is to make extensive filed visits, surveying signs of bark beetle infestation such as observing the powdery dust of feeding beetle outside the bark of the infected trees (Fettig & Hilszczański, 2015). This conventional method of involving physical travel is likely to overlook bark beetle infestation sites and thus are highly unpredictable (Hlásny et al., 2019). Because, such traditional methods to identify bark beetle infestations are costly and challenging to cover vast areas of forest (Wulder et al., 2005), and efficient remote sensing method is an appropriate solution. Therefore, remote sensing methods to find out bark beetle outbreaks are expected to be cost-effective and suitable considering the rapid development of earth observation technology (Carter et al., 1998; Chen & Meentemeyer, 2016).

1.5. Optical remote sensing data used for the bark beetle study

Numerous remote sensing studies have used a variety of optical sensors for identifying the pest infestation in the forests. Carter et al. 1998 used NDVI based on airborne sensor imagery obtained over Ouachita National Forest, to classify beetle damage of *Pinus echinatn*. Coops et al. (2006) used QuickBird multi-spectral imagery to classify mountain pine beetle attack and validated significant relationship ($r2=0.48$) with independent field data in British Columbia. Again, in British Columbia, the high spectral resolution of EO-1 Hyperion based moisture indices was used to identify bark beetle affected forests (White et al., 2007). Recently Abdullah et al. (2019a) examined that the spectral vegetation indices of Sentinel-2 (67%) are more accurate in detecting green attack than Landsat-8 (36%). Similarly, Yang (2019) used Sentinel-2 to effectively map bark beetle infestation in Sweden. However, there is a limited number of studies focused on using radar satellite images for forest pest infestations. Senf et al., (2017) reviewed SAR application studies and recommended to widen the studies to exploit spatial and temporal analysis for bark beetle infestation of spruce forests.

1.6. Temporal analysis of remote sensing methods applied for forest pest study

Latifi et al. (2014) combined 11-year time series LANDSAT and SPOT scenes and performed object-based classification which resulted in a clear separation of non-infected and dead trees in the Bavarian Forest National Park in Germany. Hais et al. (2016) analyzed the variables for spatially predicting the risks of bark beetle disturbance within the central part of the Šumava Mountains in central Europe using a time series of 16 Landsat TM images. Meddens et al. (2013) compared the single date and multi-date methods using Landsat imageries and found that multi-temporal is more accurate to detect at intermediate levels of tree mortality and single data image to be better at higher tree mortality. Similarly, Yang (2019) also used a multitemporal classification method using the Sentinel-2 time series to detect bark beetle infestation in Sweden. These studies affirm that temporal profile methods possibly can identify the trajectory of infestations in the forests over time. However, no study has ever attempted to explore SAR temporal profiling for the identification of the bark beetle infestations. This study will consider leveraging the temporal analysis of Sentinel-1 SAR data for differentiating the healthy and infected spruce trees.

1.7. Synthetic Aperture Radar (SAR) data used for bark beetle study

Studies have explored the utility of active synthetic aperture radar (SAR) sensors for studying bark beetle infestation. Ortiz et al. (2013) found that the combination of TerraSAR-X and RapidEye produced more accurate results than RapidEye alone in identifying the green attack in Germany. Rüetschi et al. (2019) successfully used Sentinel-1 SAR to assess the rapid windthrow of forest trees in both Switzerland and Germany and found that windthrow leads to bark beetle outbreaks by weakening the host trees. Likewise, XUE et al. (2018) found that Sentinel-1 SAR backscatter can be used to map pine forests affected by shoot beetles in the Yunnan area, China. Most of these studies show the ability of SAR backscatter to identify the affected areas of bark beetle infestations in the spruce forests. Tanase et al., (2018) reported a change of − 1.0 dB difference of radar change ratio between pre-disturbance and post-disturbance done by wind and insect to the forest and radar backscatter coefficients. Hollaus & Vreugdenhil, (2019) also found a difference of approximately 1 dB backscatter value in the Sentinel-1 signals of the healthy trees of 2015 and the bark beetle infected spruce trees of 2017 and recommended the study to explore the use of dense temporal resolution.

Considering the aforementioned studies, it is likely that Sentinel-1 SAR could perhaps be feasible to differentiate the bark beetle infestations of trees in the spruce forests. However, most of the past studies that used SAR focused solely on image classification methods for differentiating between the healthy and bark beetle infected spruce trees. There are inadequate studies that have investigated the methods to use Sentinel-1C-band SAR data for differentiating between the healthy and bark beetle infected spruce trees. To understand how Sentinel-1 C-band backscatter compares between the healthy and infected spruce trees, their backscatter response will be explored in this study.

1.8. Potential of Sentinel-1 C-band SAR for differentiating between healthy and bark beetle infected spruce trees.

The Sentinel-1 C-band SAR data has potential to serve the dearth of information on beetle infestation which is critical for mitigation strategy, to eliminate the infected trees before further spreading occurs and cause additional widespread devastation to larger forested areas (Hlásny et al., 2019; Wermelinger, 2004). Sentinel-1 data has only C-band SAR which has limitations for estimating forest biomass due to its limited capacity to penetrate through the vegetation (GFOI, 2018; Laurin et al., 2018). Nevertheless, C-band may still provide useful canopy information for differentiating healthy and bark beetle-infected trees, which the signal does not need deep penetration. Therefore, remote sensing methods of using Sentinel-1 SAR data has the potential to identify infected spruce trees. If the methods of using Sentinel-1 SAR to differentiate between the healthy and infected tree is feasible, then it would be more cost-effective than other commercial remote sensing sensors. Besides, the availability of high temporal frequency, Sentinel-1 SAR has the advantage of collecting data irrespective of time and weather limitation over large geographic and temporal scales (ESA, 2019).

The potential of Sentinel-1 data to differentiate between healthy and infected spruce trees is expected to provide vital information required for effective forest management and sustainable certification of forest management. For example, the spatial information on bark beetle infestation would guide forest managers to decide strategic sanitation operations. Also, a sustainable certification institution can use to assess whether the forest managers followed a timely sanitation operation to be granted a sustainable status. The public finance can use the information to corroborate bark beetle damage compensation schemes. For this purpose, it is important to examine if Sentinel-1 SAR could be used to differentiate between the healthy and bark beetle infected spruce trees.

The systematic changes in the physiological process of the host trees to counteract bark beetle damage are expected to allows remote sensing sensors instruments to capture data on the symptoms of bark beetle incidence in the forest (Egan et al., 2016; Overbeck & Schmidt, 2012). The leaves of infected host trees showed the effect of water and nutrient stress after the disruption of inner bark tissues by the beetles (Chinellato et al., 2014; Coops et al., 2006). Studies have also confirmed that remote sensing sensors are sensitive to the change in leaf pigments, tissue structure, and amount of water content of leaves of the trees (Bright et al., 2013; Darvishzadeh et al., 2019; Fassnacht et al., 2014; Wulder et al., 2005). Radar dielectric constant properties of dry vegetation are comparatively lower than the living vegetation due to more water content in living vegetation (Attema & Ulaby, 1978; Öquist & Huner, 2003). Since the higher water content of the living vegetative parts influences higher dielectric constant which in turn influences more backscatter response, healthy spruce trees possibly will show higher backscatter response than the infected spruce trees (Öquist & Huner, 2003). Therefore, Sentinel-1 C-band SAR is expected to show the change processes of the healthy tree into an infected spruce tree as its foliage sheds off and the water or nutrients supply gets disrupted (Chen & Meentemeyer, 2016). Figure 1 shows the conceptual diagram for exploring the potential of Sentinel- 1 C-band SAR to differentiate between the healthy and infected spruce trees.

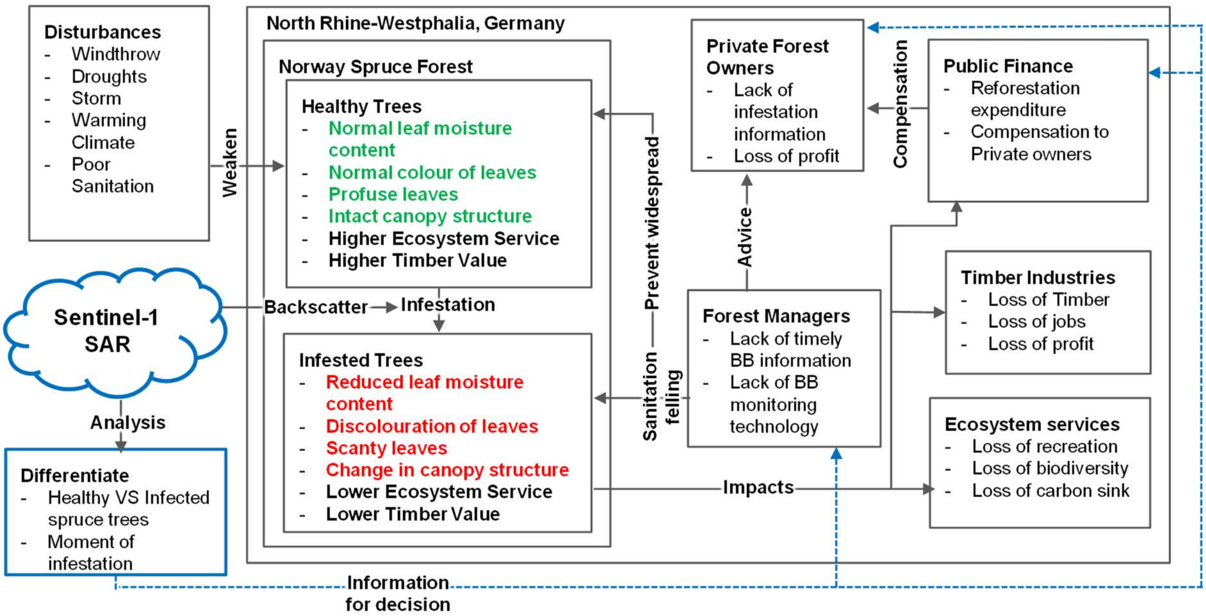

Figure 1. The conceptual diagram for differentiating between the healthy and bark beetle infected spruce trees. Red and green colour indicates the variable quantifiable by Sentinel-1 SAR remote sensing data. The dotted blue line indicates the possible application of the study outcomes.

1.9. Problem Statement

Hlásny et al. (2019) emphasized the need for a user-friendly and cost-efficient remote sensing technology for monitoring bark beetle infestation to guide forest management. Similarly, Morris et al. (2017) also documented the urgent requirement of cost-effective and efficient remote sensing method to improve bark beetle detection and mapping that can monitor over large geographic and temporal scales. Moreover, it is a priority research problem unanimously identified by the ecologists, land managers and social scientists from North America and Europe (Morris et al., 2017). Current methods of identifying the bark beetle infestation are physically challenging and resource-intensive (Fettig & Hilszczański, 2015). They include the visual field surveys, the use of sniffer dogs, and the use of costly optical and SAR remote sensing data (Hlásny et al., 2019). There is no clear understanding of the methods to use Sentinel-1 C-band SAR for differentiating healthy and infected spruce trees as none of the previous studies has reported on it conclusively. Therefore, this study considered to determine the applicability of the Sentinel-1 C-band SAR data and explore the method to differentiate between the healthy and bark beetle infected spruce trees.

1.10. Objectives and research questions

The study aims to determine the applicability of the Sentinel-1 data and explore the methods to differentiate between the healthy and infected spruce trees. The difference in Sentinel-1 SAR signals will be compared between healthy and infected spruce trees statistically. The temporal analysis will be performed to examine the difference in the time series patterns between the healthy and infected spruce trees.

Objective 1: To find out the possibility of single time snapshot image of Sentinel-1 SAR to differentiate the healthy and infected spruce trees.
Research Question 1: Does the SAR backscatter coefficients of healthy and infected spruce trees differ significantly?
H0: There is no difference in the SAR backscatter coefficients of healthy and infected spruce trees.
H1: There is a significant difference in the SAR backscatter coefficients of healthy and infected spruce trees.

Objective 2: To explore temporal profiling method using Sentinel-1 SAR signals to differentiate a healthy and infected spruce tree.
Research question 2: How does the temporal profiling technique with Sentinel-1 SAR help differentiate a healthy and an infected spruce tree?

2. MATERIAL AND METHODS

2.1. Study Area

The study area falls inside the northern part of Eifel National Park (ENP) which is located in the North Rhine-Westphalia state of Western Germany, between 6°23'05.08" E to 6°34'38.70" E longitude and 50°33'09.68" N to 50°38'58.06" N latitude (see Figure 2.). The study area has about 4284 hectares of the ENP's coverage. This portion of ENP was selected as the study area because the bark beetle infected spruce trees were not removed immediately within the national park jurisdictions, unlike the forested area outside park regulation. Eifel National Park was formerly a military training ground before it was established in 2004 and then the landscape was left to natural processes where large patches of spruce forests are affected by bark beetle infestation (Schmiedel, Goedecke, & Bergmeier, 2019). Therefore, the presence of standing infected spruce trees inside the ENP was found appropriate for obtaining samples of the infected spruce trees for this study purpose.

Eifel National Park has gentle topography characterized by rolling plateaus and interspersed by running streams. The elevations of the area range from 185 to 630 m and has an oceanic climate covered by both deciduous and coniferous forests (Heine et al., 2019; Schmiedel et al., 2019). Major tree species are European beech (*Fagus sylvatica),* Pedunculate oak (*Quercus robur*), Norway spruce (*Picea abies*) and Scots pine (*Pinus sylvestris*). In 2018, spruce forests experienced a traumatic incidence of heavy infestation by bark beetles and are expected to further deteriorate in 2019 (Alamy Limited, 2019). Figure 2 shows the location map of the study area.

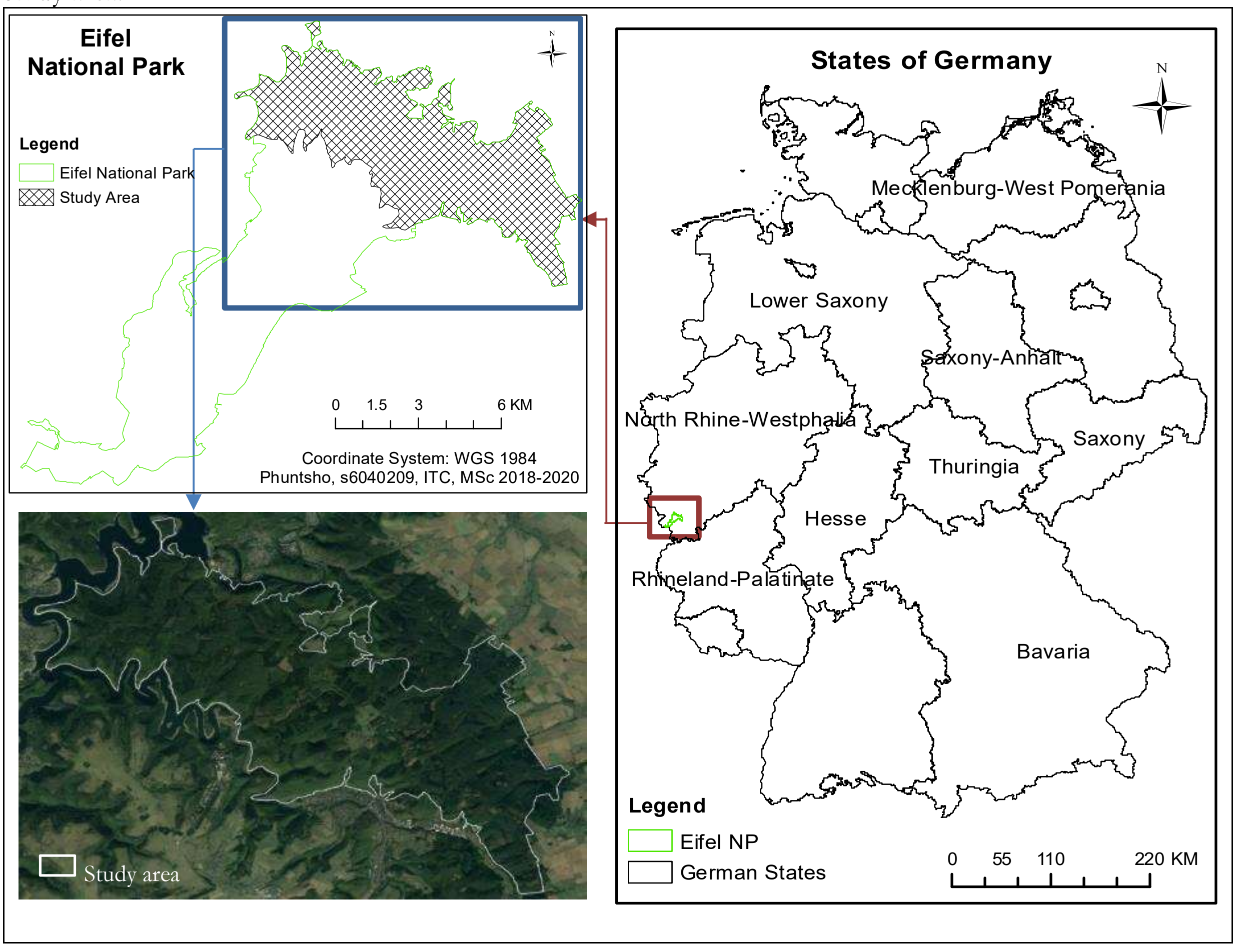

Figure 2. Map showing the location of the study area inside the Eifel National Park (ENP), in Germany.

2.2. Sampling

Spruce tree samples for both healthy and bark beetle infected spruce trees were necessary to obtain their corresponding SAR signals observed by the Sentinel-1 images. Since it was not allowed to collect field GPS coordinates of the samples inside the national park, high-resolution Google Earth imagery was used as the basis to obtain the samples of the healthy spruce trees as well as the infected spruce trees. Few sites of the previously collected GPS co-ordinates of the bark beetle infected spruce tree were provided by GRAS GmbH, Cologne, that was located nearby the study area. These GPS coordinates of those infected spruce tree sites helped to visually relate and understand the colour, texture, and pattern of bark beetle infected spruce trees observed on the Google Earth images.

Using this visual interpretation of Google Earth images, the homogeneous samples were identified and delineated for both healthy and infected spruce forest inside the study area. The healthy spruce trees samples appeared dark green colour and smaller in crown size compared to the large crown and brighter green colour canopy of broadleaved trees. The canopy of an infected spruce tree appeared to be reddish and greyish which was assumed to be as the impact of bark beetle damage. The sample polygons of the healthy and infected spruce trees were screen digitized based on the google earth high-resolution imagery of 5 October 2018. A total of 100 sample polygons of healthy spruce trees and 107 sample polygons of infected spruce trees were delineated as key markup langue zipped (KMZ) in Google Earth. The delineated samples were then converted into shapefile format in Quantum GIS (QGIS) software (QGIS Development Team, 2020). Figure 3 shows the samples of the healthy spruce trees delineated with the green polygons and infected spruce trees delineated with red polygons inside the study area.

Figure 3. The healthy spruce trees samples delineated with green polygons and the infected spruce trees samples delineated with red polygons inside the study area.

To study the possibility of a single time snapshot image of Sentinel-1 SAR to differentiate the healthy and infected spruce trees, 20 by 20-meter healthy sample inside the 100 healthy sample polygons and 10 by 10-meter infected sample points inside the 107 infected sample polygons were laying out systematically. The healthy sample points were allocated at a greater distance than infected samples points to obtain their equal count approximately as the healthy samples were more abundantly available compared to the infected sample in the study area. It resulted in a total of 2660 sample points for the healthy trees and 2342 sample points for the infected trees (Figure 4a). Appendix B explains the detailed process of laying out and generating sample points using QGIS for both healthy and infected spruce trees.

To study the temporal analysis of the SAR backscatter response, a sample point at the centre of each polygon of both healthy and infected samples were generated (Figure 4b). The centre location of the polygon was considered appropriate for the temporal analysis of the Sentinel-1 SAR signals to avoid influence from border pixels backscatters and the uncertain time of infestation for each tree.

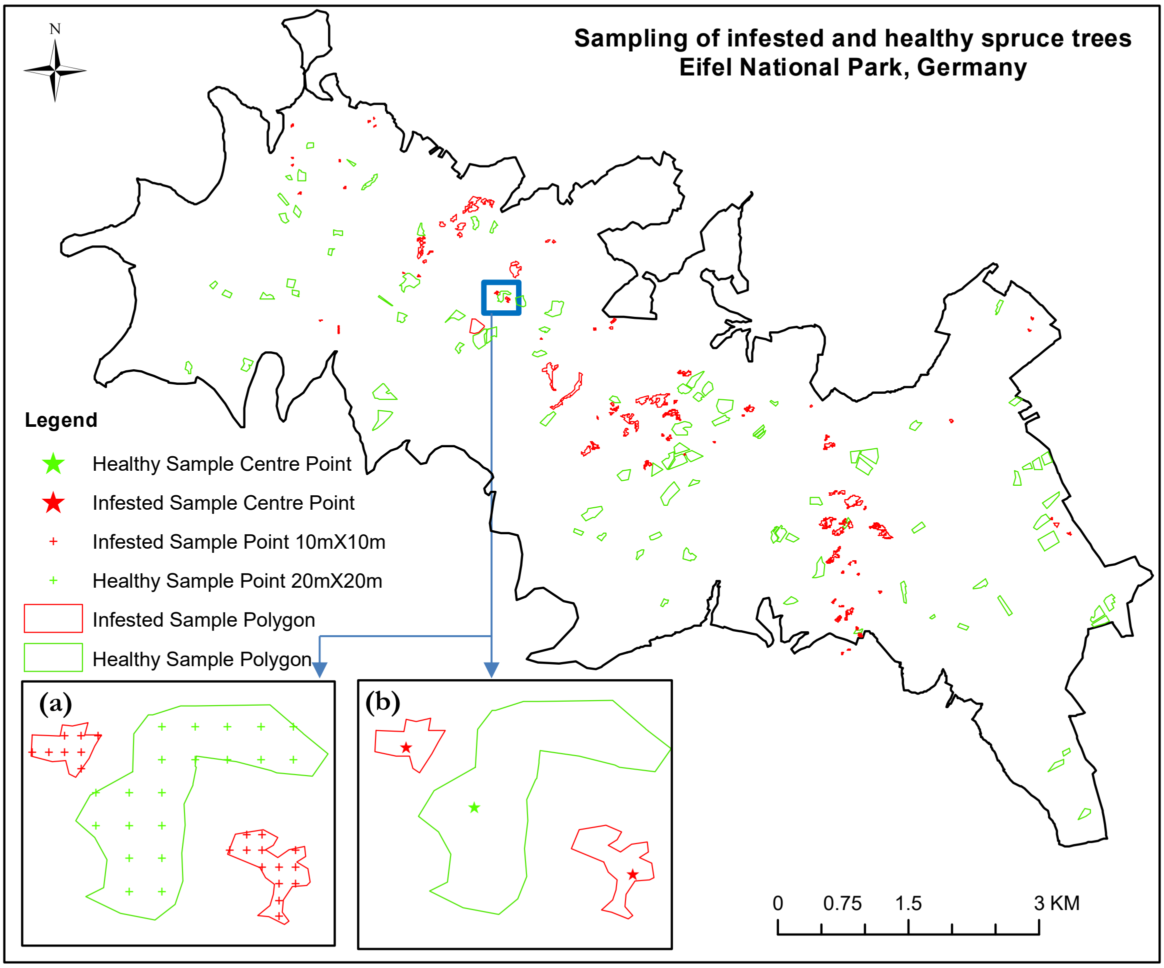

Figure 4. Sampling design for the study: (a) 20 by 20 meter distributed sample points inside the 100 healthy sample polygons, and 10 by 10 meter distributed sample points inside the 107 infected sanple polygons to analyze a single time snapshot image of Sentinel-1 SAR response. (b) A sample point at center of each polygons (both healthy and infected sample) for temporal analysis of the SAR backscatter response.

2.3. Sentinel-1 SAR imagery

Sentinel-1 is the Copernicus Programme satellite of the European Space Agency (ESA) for Synthetic-aperture radar (SAR) remote sensing. SAR is an enhanced radar technology to obtain higher spatial resolution than traditional radar data measurements of the target landscape. Sentinel-1 consists of two earth observation satellite constellations, Sentinel-1A and Sentinel-1B, launched on 3 April 2014 and 25 April 2016 respectively. They carry the C-band synthetic-aperture radar (SAR) apparatus for the collection of single or dual polarization with a revisit time of 6 days at equator. Copernicus Open Access Hub and other data providers allow to access two types of Sentinel-1 products, Ground Range Detected (GRD) and Single Look Complex (SLC). For this study, Sentinel-1 level-1 GRD products were used, covering the period from 2014 to 2019 of the study areas. Generally available SAR data of Sentinel-1 level-1 GRD products consists of VV (Vertical-Transmit and Vertical-Receive) and VH (Vertical-Transmit and Horizontal-Receive) dual-polarization channels. One additional channel was computed by calculating the ratio between VV and VH, using the band math function of the opensource Sentinel Application Platform software (SNAP) developed and distributed by ESA. Appendix C shows the screenshot of performing band math function in the SNAP.

SAR scenes were filtered, selected, and downloaded using the Alaska Satellite Facility (ASF) by restricting spatial filter criteria to the study area. Sentinel-1A satellite products were selected considering its longer period of observations that started from 2014 onwards over the Sentinel-1B satellite products which started its mission only from 2016. Level-1 GRD was considered appropriate in comparison to SLC as preprocessing steps such as scene focusing, multi-looking, and projection to ground range using an Earth ellipsoid model has been applied by the data provider. Besides, the SAR scene was filtered to ascending orbit properties to avoid mixing of the different signals due to the angle and direction of observation influenced by differences in the satellite orbital path. Appendix A listed the steps followed on filter criteria and scene properties used to download the Sentinel-1A SAR for the study.

2.4. SAR preprocessing

SAR pre-processing is an essential procedure to prepare the SAR scene into meaningful data after applying essential rectification. Sentinel-1A SAR level-1 GRD images contain radiometric bias, geometric distortion, and raw backscatter intensity. Therefore, it is necessary to enhance the SAR scene by applying suitable corrections and improvements so that the pixel values of the images correspond with the actual radar backscatter of the target surface. To tackle this, the European Space Agency (ESA) offers open-source software known as the Sentinel Application Platform (SNAP) suitable for the SAR processing.

Pre-processing of the Sentinel-1A SAR was carried out using the SNAP platform since it is free and open-source. SNAP has a neater handling capability of Sentinel-1 SAR data as it is designed purposefully for it by the data provider (ESA). Application of orbit file, removing thermal noise, radiometric calibration, terrain correction, and conversion to decibel (dB) were the preprocessing steps applied to Sentinal-1 SAR data using the SNAP batch processing option. Figure 5 illustrates the Sentinel-1 SAR data processing steps applied for all the Sentinel-1 observations from 2014 to 2019.

Figure 5. Diagram showing the Sentinel-1 SAR processing steps applied for this study.

The detailed steps and logics for performing the preprocessing steps, advocated by the data provider (ESA) are described in the following sections.

2.4.1. Apply orbit file

The satellite orbit information provided along with the SAR scenes at the time of data acquisition are generally not accurate and need to be refined at later stages when precise orbit information becomes available. Metadata of the scenes are updated by obtaining the precise satellite position and velocity information which usually becomes available approximately after 2 weeks of data acquisition. SNAP graph builder was used to automatically check the availability of the precise orbit file archived in the online database and accordingly applied to the Sentinel-1 SAR scenes. The precise orbit file information also improves the SAR data analysis that requires satellite information in all other SAR processing steps.

2.4.2. Thermal noise removal

During the process of the Sentinel-1 SAR satellite image acquisition, the background energy created by imaging receiver instruments gets incorporated as thermal noise into the radar backscatter signals. To remove the thermal noise, the SNAP platform was used to apply thermal noise removal to Sentinel-1A SAR data of this study. This process uses the noise lookup tables provided with the data and enhances the SAR signals by avoiding skewed radar reflectivity.

2.4.3. Radiometric calibration

Radiometric calibration refers to the processes of refining the radar signals so that the image pixel value associates directly to the characteristics of the scene backscatters. The strength of the collected radar signal depends on considerations such as a receiver or antenna gains, system loss owing to the relative positioning of the resolution, and sensor that introduces significant radiometric biases in the SAR image. Radiometric calibration is performed by computing the backscatter coefficient known as sigma nought (Sigma0). This fundamental processing of SAR calibration was also successfully performed along the chains of the graph builder process for the SAR scenes of this study.

2.4.4. Geometric correction

Geometric correction or some times referred to as terrain correction is the process of orienting the SAR signal coordinate geometry system to an ortho-corrected coordinate system. The SAR system has side looking geometry system at the time of SAR scene acquisition where every landscape SAR signal obtained is mapped on the slant range domain that does not conform with the standard cartographic system. Therefore, terrain correction was also inevitably performed using a graphical builder in the SNAP platform for the SAR scenes of this study, to convert from slant range to ground range geometry into a defined coordinate system.

2.4.5. Conversion to decibel (dB)

The pixel values of SAR images after radiometric calibration are transformed into the SAR signals in terms of SAR backscatter intensity. SAR backscatter intensity of image pixel is the percentage of microwave energy returned from the target surface which depends on the properties of surface such as shape, size, and moisture content as well as the properties of sensor systems such as incident angles of the radar, polarization. Therefore, SAR scenes were converted to a quantifiable physical quantity called the backscattering coefficient measured in decibel (dB) units using the graph builder in the SNAP platform. The values of SAR backscatter normally range from +5 dB for the bright surface to -40 dB dark areas. The distribution between the SAR backscatter intensity and converted backscatter coefficient in dB units were compared (Figure 6 & 7.) and showed a normal Gaussian distribution after conversion to dB.

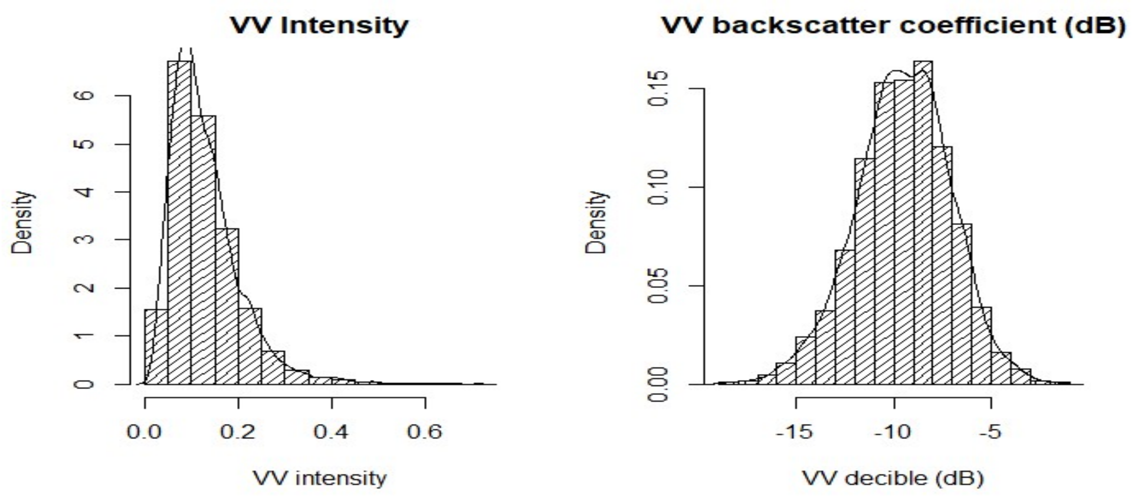

Figure 6. Histogram showing the distribution of SAR backscatter intensity and backscatter coefficients

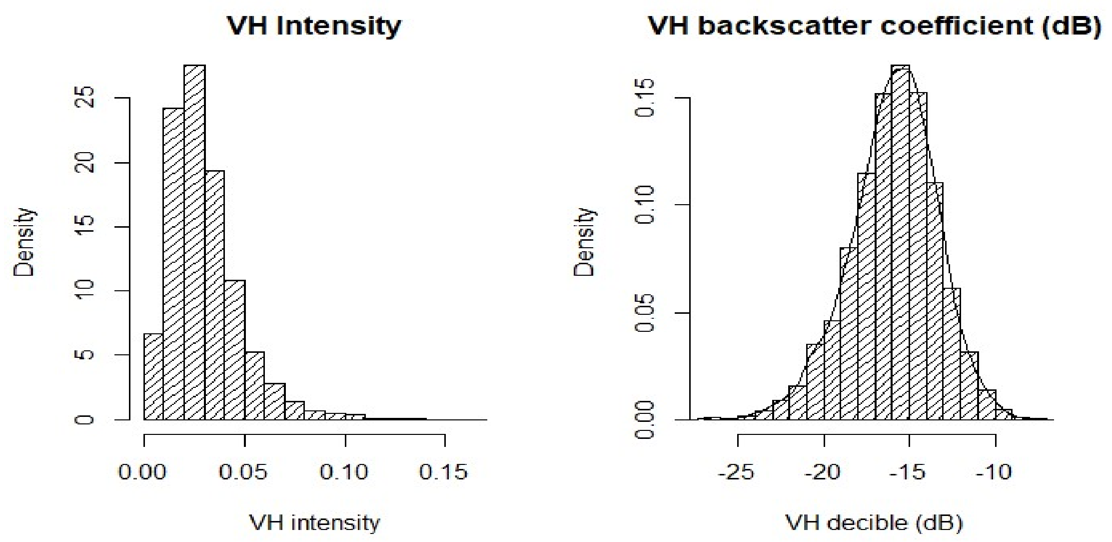

Figure 7. Histogram showing the VH SAR intensity and backscatter coefficients

2.5. Comparing the statistical difference of Sentinel-1 SAR backscatter response between healthy and infected spruce trees based on a single time snapshot of an image

To study the possibility of a single time snapshot image of Sentinel-1 SAR to differentiate the healthy and infected spruce trees, the SAR backscatter response between healthy and infected spruce trees were analysed. For this purpose, a single time snapshot of the Sentinel-1 images of the study area was selected for the analysis. Pre-processed Sentinel-1 SAR image acquired on 02 October 2018 over the study area was chosen to analyze the SAR signals differences of each polarization between the healthy and infected spruce trees. The SAR image acquired on 02 October 2018 was found to be the closest with the Google Earth image acquisition date on the 5 October 2018 which was used for sampling the healthy and infected spruce trees.

The Sentinel-1 SAR backscatter coefficient values of VV, VH, and VV/VH ratio polarization channels were extracted using 2660 healthy tree samples points and 2342 infected tree sample points. SNAP software was used to perform the SAR backscatter coefficient values corresponding to each location of the sample points. Appendix D shows the detail steps of extracting the SAR signal using the SNAP platform.

To study if the Sentinel-1 SAR backscatter coefficients response of a healthy differ from that of an infected tree significantly, the distribution and statistical student's t-test of the mean of the backscatter response were performed. To graphically analyze the distribution of Sentinel-1 backscatter response between healthy and infected spruce trees, the histogram illustrating the distribution was prepared based on the SAR signals extracted using the healthy and infected sample points. The histogram was prepared using R-statistical and Microsoft Excel worksheets to visually compare the frequency distribution of the SAR signal between the healthy and infected spruce for each SAR polarization channels. An independent student t-test was performed between the mean of the backscatter response of healthy and infected trees separately for each SAR polarization channels using the R-statistical software. Statistical variance test and normal quantile plots were also carried out between the healthy and infected spruce trees sample data to check if the samples meet the assumptions of independent student t-test. Appendix E details the process of checking the assumptions for the independent two-sample t-test.

2.6. Developing the temporal profile using Sentinel-1 SAR backscatter response of the healthy and infected spruce trees based on the time series images

The SAR temporal profiling method was explored to study if the temporal profiling method is applicable to differentiate a healthy and infected spruce tree using their time-series Sentinel-1 backscatter values. The temporal profile was developed using the SAR backscatter response extracted using the centre point of each polygon samples of both healthy and infected spruce trees. R statistical software and Microsoft Excel was used to build a time-series graph based on the SAR backscatter values to illustrate the temporal pattern graphically. The temporal pattern is expected to visually display the difference between healthy and infected spruce trees.

A representative temporal profile for healthy spruce trees was prepared based on the average backscatter values of the healthy polygon samples. The representative temporal profile was developed visually display the typical characteristics of SAR backscatter response of the healthy spruce trees. This representative healthy temporal profile is expected to show the sensible annual pattern of the healthy spruce trees as it was based on the average SAR signals of all the healthy trees sample polygons. Therefore, such a typical representation of healthy spruce trees would enable us to form a benchmark to compare with the temporal profile of the infected spruce trees.

The temporal profile for infected spruce trees was developed based on the time series SAR backscatter response at the centre point of infected sample polygons. However, it is not logical to develop a representative temporal profile for the infected spruce tree as the time of the infestation of each tree may differ from one another. Therefore, in the case of the infected temporal profile, every pixel on SAR imagery or each spruce tree in the forests may show localized patterns according to the time and location at which bark beetle infestation might have happened. Appendix H shows the R scripts used for the temporal analysis of the SAR backscatter response of healthy and infected spruce trees.

2.7. Applying Adaptive Savitzky-Golay filter (ASAVGOL) to enhance the pattern of the temporal profile

The Adaptive Savitzky-Golay filter (ASAVGOL) algorithm is based on the least square computational processes to correct inconsistent time-series data by swapping each data values at a consecutive linear combination over a time window (Beltran-Abaunza, 2009). The ASAVGOL filter is expected to enhance the annual pattern of the temporal profiles. Since SAR backscatter responses are prone to inherent noise such as thermal noise, radar radiometry errors, and landscape topography influences, it would be appropriate to apply to the representative healthy temporal profile (Ahern, Leckie, & Drieman, 1993; Rüetschi, Schaepman, & Small, 2017; Saatchi et al., 2013). As the representative healthy temporal profile is based on the averaged values of healthy SAR backscatter values, ASVGOL filter is expected to the pattern of the healthy spruce trees. Accordingly, the ASAVGOL filter was applied to remove inconsistent time-series SAR backscatter values of the healthy trees averaged across the timestamp.

The correction factors were obtained for each of the timestamps by computing the difference between the ASAVGOL filtered backscatter response and its raw backscatter values based on the average data of the healthy spruce trees. The correction factor was then applied to the infected temporal profile linking each timestamp to remove their time-series inconsistency of the backscatter response. The output after applying the correction factor to the infected temporal profile is expected to remove the localized noised effect and produce the true backscatter response that shows the properties of the actual landscape surface.

2.8. Verifying temporal profiling method to differentiate between healthy and infected spruce trees

To study the ability of Sentinel-1 SAR backscatter temporal profiling method to differentiate between healthy and infected spruce trees, an independent site outside the study area using a different set of Sentinel-1 SAR temporal profile analysis was performed. The bark beetle infestation period of the independent site was deduced from two consecutive google earth images acquisition dates between 20 April 2018 and 22 April 2019 (Figure 8). An infected tree location was randomly chosen where the time series Sentinel-1 SAR backscatter values were using the Google Earth Engine platform (Gorelick et al., 2017). Based on these time series SAR backscatter values, a temporal profile of that location was prepared to examine the pattern difference before and after the infestation period. The blue star marked on the right side of the image in Figure 8 shows the location of the site that was used to prepare a temporal profile to verify the period of bark beetle infestation. Appendix G shows the Google Earth Engine java scripts used for this exercise.

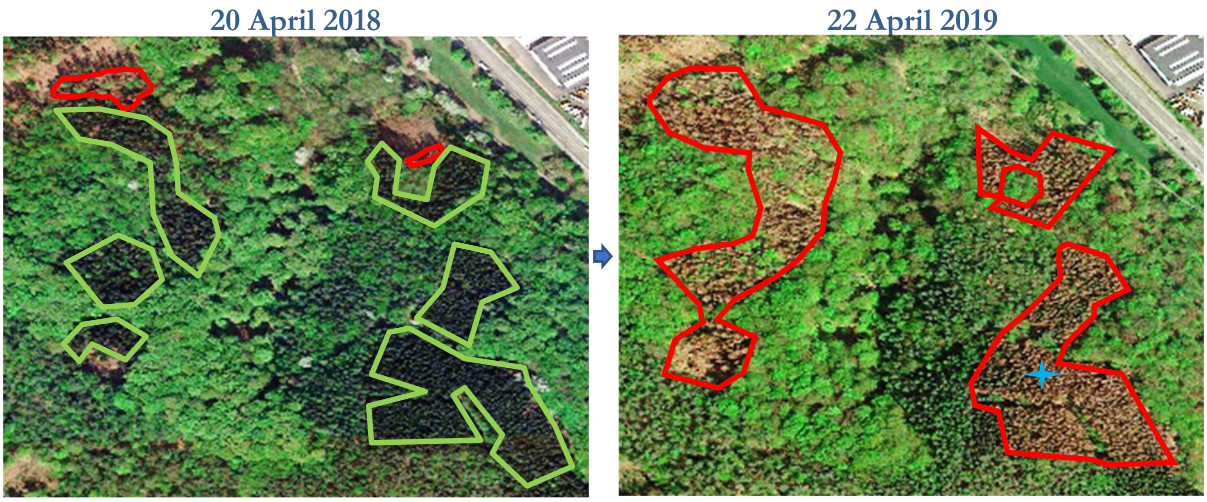

Figure 8. A spruce forest site in Rheinbrohl, Germany, showing the evidence of time taken by a bark beetle infestation process that can be visually interpresteed from healthy to an infected spruce tree. Green polygon show the healthy spruce trees and red polygon shows the bark beetle infected spruce tree,.

2.9. Exploring the influence of rainfall on the temporal profile pattern of the SAR backscatter response

Studies have found that rainfall is one of the factors that cause the change of the SAR backscatter (Rüetschi et al, 2017; Saatchi et al., 2013). It is essential to remove the backscatter outlier values influencing the temporal profile pattern that is affected by rainfall events (Tanase et al., 2018). To examine the influence of the rainfall on the backscatter values, the precipitation of local station data was compared with the backscatter response of the samples. The rainfall data were obtained from the local weather station of the study area. The precipitation data of Mannebach/Eifel weather station located at Rheinland-Pfalz was download from the data distribution websites. Accordingly, the precipitation was plotted alongside the time-series graph of the Sentinel-1 SAR backscatter response to explore for any link between backscatter coefficients values and precipitation.

2.10. Sentinel-2 Optical imagery

As per ESA, Sentinel-2 consist of two polar-orbiting sun-synchronous satellites, Sentinel-2A and Sentinel-2B launched on 23 June 2015 and 7 March 2017, respectively. Sentinel-2 acquires optical imagery at a high spatial resolution at 10 m (four visible and near-infrared bands), 20 m (six red edge and shortwave infrared bands), and 60 m (three atmospheric correction bands) and covers a swath width of 290 km.

Sentinel-2 optical images were considered to compare the possibility of differentiating the healthy and bark beetle infected spruce trees between Sentinel-1 SAR images and Sentinel-2 optical images. Studies have found that red-edge and SWIR spectral information from optical satellite imageries can be used for the detection of bark beetle-infected (Abdullah et al., 2018; Abdullah et al., 2019b). Further, Abdullah et al. (2019a) found that the red-edge based indices and water-related indices of Sentinel-2 bands can successfully separate healthy from infected trees. Besides, Yang, (2019) also used a combination of vegetation indices of Sentinel-2 imagery for the classification of bark beetle infestation and healthy forest areas. So, the Sentinel-2 optical imagery was also downloaded and processed for this study area from 2014 to 2019.

2.10.1. Sentinel-2 Pre-processing

Sentinel-2 image pre-processing was automatically performed using the sen2r platform (Ranghetti & Busetto, 2019). Sen2r platform is a package developed for the R Project for Statistical Computing software. Sen2r had downloaded and pre-processed all the Sentinel-2 satellite imageries required for this study. Sen2r applied atmospheric correction of the Sentinel-2 scenes and produced bottom-of-atmosphere reflectance. After visual inspection, only 23 of Sentinel-2 images observed by both Sentinel-2A and Sentinel-2B from 2014 to 2019 were found to be cloud-free and usable for analysis.

2.10.2. Preparing the Sentinel-2 NDRE Index

Sen2r pre-processed Sentinel-2 scenes were imported into the SNAP platform for computing spectral indices. SNAP platform was preferred since its graph builder allows automatic batch processing of all the time-series images iteratively. The Sentinel-2 image indices based on red-edge spectral bands of Sentinel-2 were prepared for temporal profiling to differentiate between a healthy and infected spruce trees to see how it compares with that of SAR temporal profiling. Normalized Difference NIR/Red-edge (NDRE) was calculated using the band math function of SNAP with the Sentinel-2 scenes of the study area. NDRE estimates the chlorophyll content of the leaves which can be used as an indicator of vegetation health (Frampton et al., 2013). NDRE was computed based on the formula shown in Equation 1.

Equation 1. The formula used for computing the NDRE index.

$$NDRE = \frac{NIR - Red\ edge}{NIR + Red\ edge}$$

2.11. Developing the temporal profile using the Sentinel-2 NDRE index of the healthy and infected spruce trees based on the time series images

The temporal profile was also developed using the Sentinel-2 NDRE index using the centre point of each polygon samples of both healthy and infected spruce trees. SNAP platform was used to extract the NDRE spectral index values using its batch processing functions based on the centre of the sample polygons. Similar to SAR profiling techniques, R statistical software and Microsoft Excel was used to build a time-series graph based on the Sentinel-2 NDRE index values to illustrate the temporal pattern graphically. The Sentinel-2 NDRE index-based temporal were developed for both healthy and infected spruce trees.

3. RESULTS

The findings of the statistical difference and temporal analysis are presented to determine the applicability of Sentinel-1 SAR and a method to differentiate between the healthy and infected spruce trees.

3.1. The distribution and the statistical difference of Sentinel-1 SAR signal response between healthy and infected spruce trees

There is a substantial overlap in the distribution of Sentinel-1 SAR backscatter response of a healthy and infected spruce trees across all the channels of the polarization (Figure 9a-d). However, there is a slight difference in the location of the mean SAR backscatter response between the healthy and infected trees as indicated by the whisker boxplot (Figure 9d).

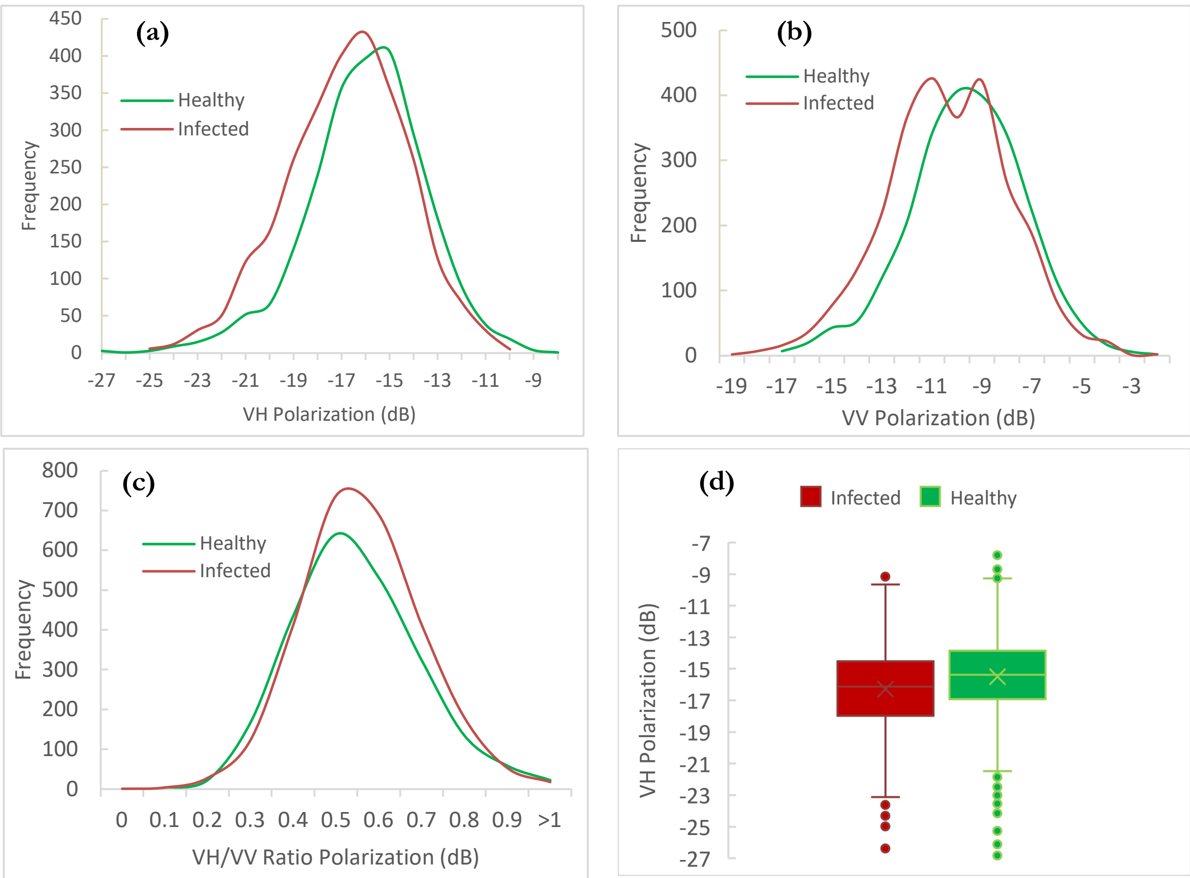

Figure 9 (a -d): Comparing the distribution of Sentinel-1 SAR backscatters response between healthy and infected trees across (a) VH polarization, (b) VV polarization, (c) VV/VH polarization and (d) VH polarization boxplot.

An independent two-sample t-test showed that there is a significant difference (p <0.05) in the mean Sentinel-1 SAR backscatter response between healthy tree (n = 2660) and infected tree (n = 2342) of spruce trees. Table 1 shows the p-values of the t-test results of different polarization.

Table 1. Two-sample independent t-test comparing healthy and infected spruce trees for different polarizations.

Sigma Polarization	t-statistics	p-value	Mean Healthy Trees (dB)	Mean Infected Trees (dB)	Difference Between Healthy & Infected (dB)
VV (dB)	10.673	2.2e-16	-9.13	-9.86	- 0.73
VH (dB)	11.410	2.2e-16	-15.49	-16.29	- 0.80
VV/VH (dB)	-3.3345	0.00086	0.59	0.60	- 0.01

3.2. Temporal profile of the healthy spruce tree shows an annual seasonal pattern

The Sentinel-1 SAR temporal profile of the healthy spruce tree shows an annual seasonal pattern. The seasonal pattern a healthy temporal profile is graphically indicated by a wave across the time series (Figure 10). The sinusoidal pattern peaks higher in the summer the months of June-July and dips lower the winter months of January- February throughout the annual cycle. The temporal profile shown in Figure 10 is based on an averaged values of all healthy SAR backscatter samples at each timestamp expected to be the representative profile of typical healthy trees. The green dotted line indicates the raw backscatter time-series signals and the green thicker line indicate the Adaptive Savitzky-Golay filter (ASAVGOL) enhanced the temporal profile pattern. The ASAVGOL filter has removed the extreme variability of the backscatter response of the healthy trees.

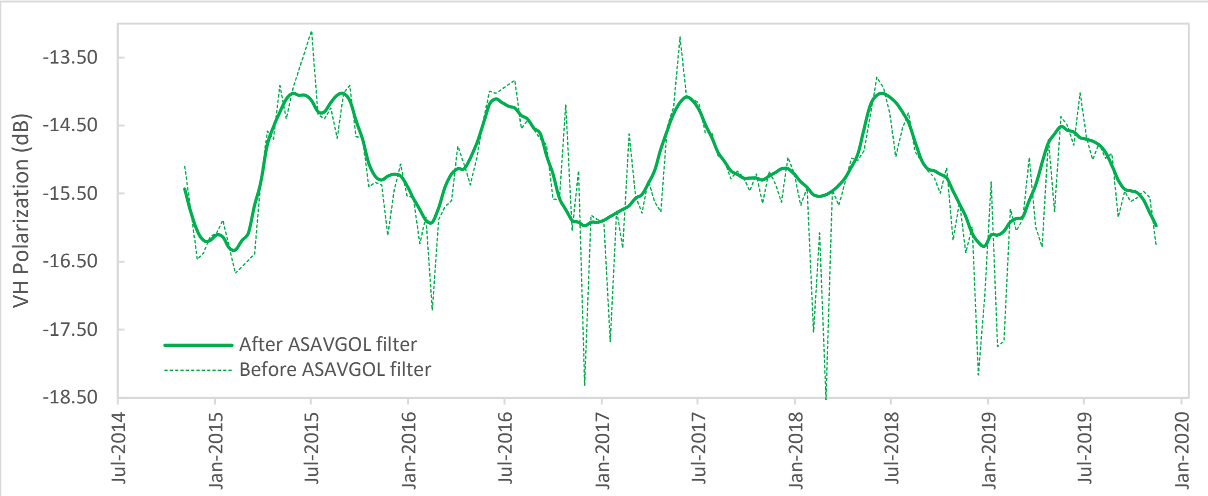

Figure 10: The Sentinel-1 SAR backscatter temporal profile of a healthy trees. The green dotted line indicate the raw backscatter time series signals and the green thicker line indicate the Adaptive Savitzky-Golay filter (ASAVGOL) enhanced profile pattern.

3.3. Temporal profile of the infected spruce tree show irregular pattern

The Sentinel-1 SAR temporal profile of the infected spruce tree shows an irregular pattern. Since the time of the infestation of each tree may differ from each other, a representative profile for the infected tree is not logical. One of the temporal profile of an infected tree (the sample no. 42 Figure 11) was randomly selected to illustrate its pattern. There is no clear association between the seasons and the pattern for the sample no. 42 (Figure 11). In Figure 11, the seasonal pattern stops after the end of the year 2015 and then irregular pattern follows until the end of the year 2019 assumed as the impact of a bark beetle damage. The red dotted line indicates the raw backscatter time-series signals and the red thicker line indicate the Adaptive Savitzky-Golay filter (ASAVGOL) filtered temporal profile pattern (Figure 11).

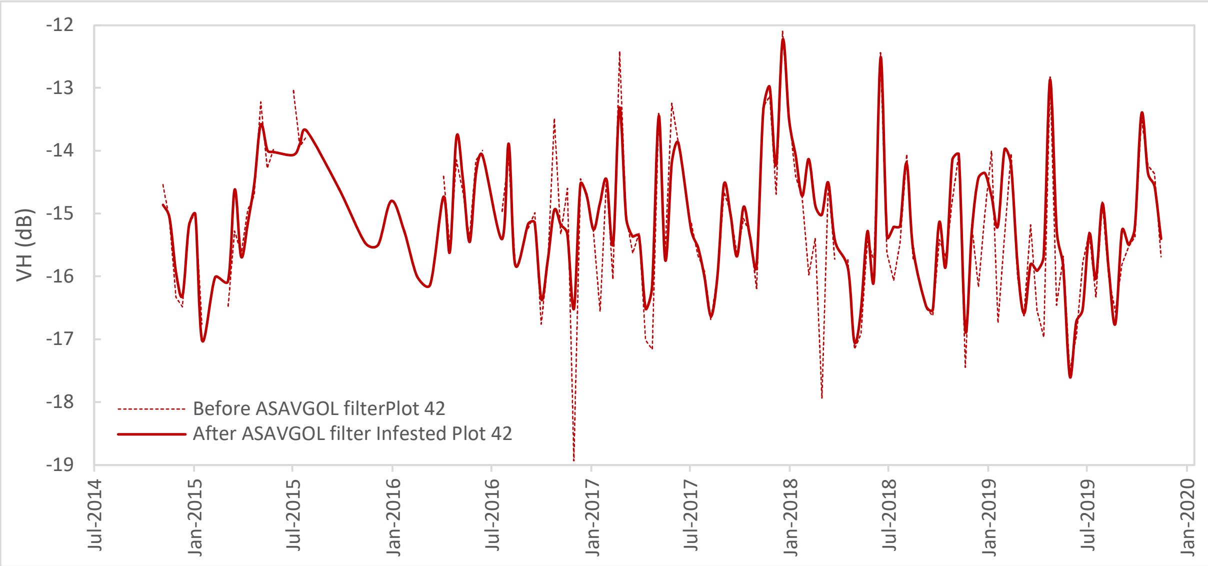

Figure 11: Sentinel-1 SAR temporal profile of the infeted spruce trees of the sample polygon no. 42 at the centre pixel location. The red dotted line indicate the raw backscatter time series signals and the red thicker line indicate the Adaptive Savitzky-Golay filter (ASAVGOL) enhanced backscatter values.

3.4. The difference in the temporal pattern of a healthy and infected spruce trees

The temporal profile pattern overlaid with both ASAVGOL cleaned SAR backscatter response of the healthy and infected spruce trees shows the difference of their profile pattern that enables to differentiate as a healthy and infected spruce tree (Figure 12). The transition from an annual seasonal pattern to an irregular pattern on a temporal profile (approximately in January 2016) can be assumed as the moment of a bark beetle infestation that facilitates to differentiate between a healthy and infected spruce tree (Figure 12).

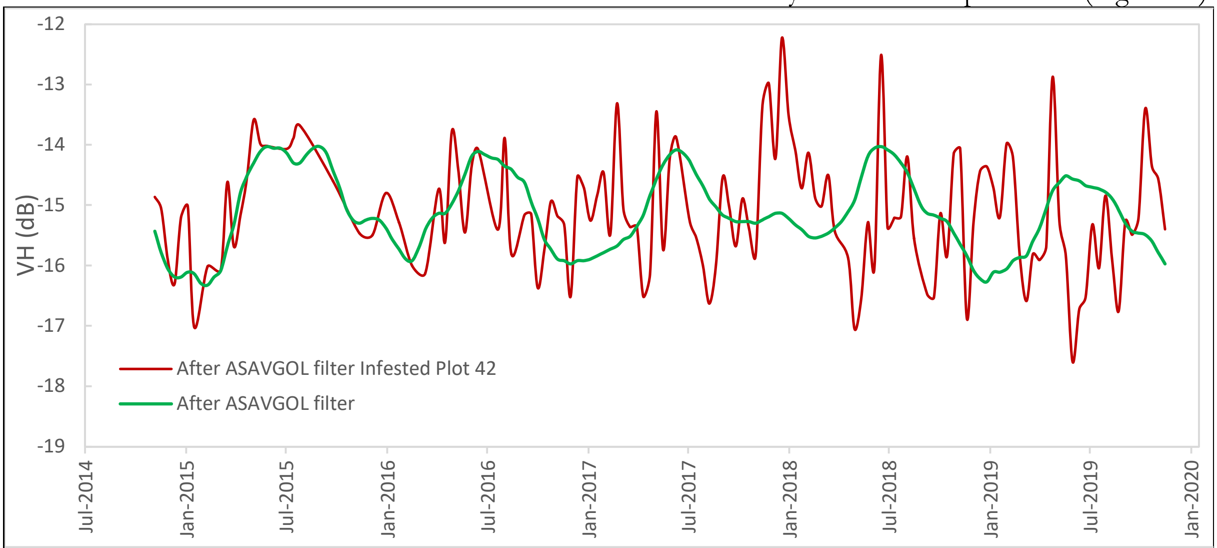

Figure 12: The ASAVGOL cleaned temporal profile pattern of a healthy (red) and infected (green) spruce trees.

3.5. Verification of the moment of infestation with the temporal profile of an independent site

The SAR temporal profile of a spruce forest site independent of the study area samples proves that the moment of bark beetle impact on the spruce trees can graphically display and show coherently the period of infestation. The predetermined period was based on the Google Earth image that showed a visible change of spruce trees canopy discolouration between 22 April 2018 and 24 April 2019 (Figure 8). Coinciding with the same predetermined period, the SAR temporal profile shows a pattern of the change from regular sinusoidal to the irregular pattern between July 2018 and January 2019 (Figure 13). Therefore, this temporal profile of an independent site with independent Sentinel-1 SAR analysis performed through Google Earth Engine (Gorelick et al., 2017), confirms the robustness of the SAR temporal profiling technique to differentiate between the healthy and infected spruce trees.

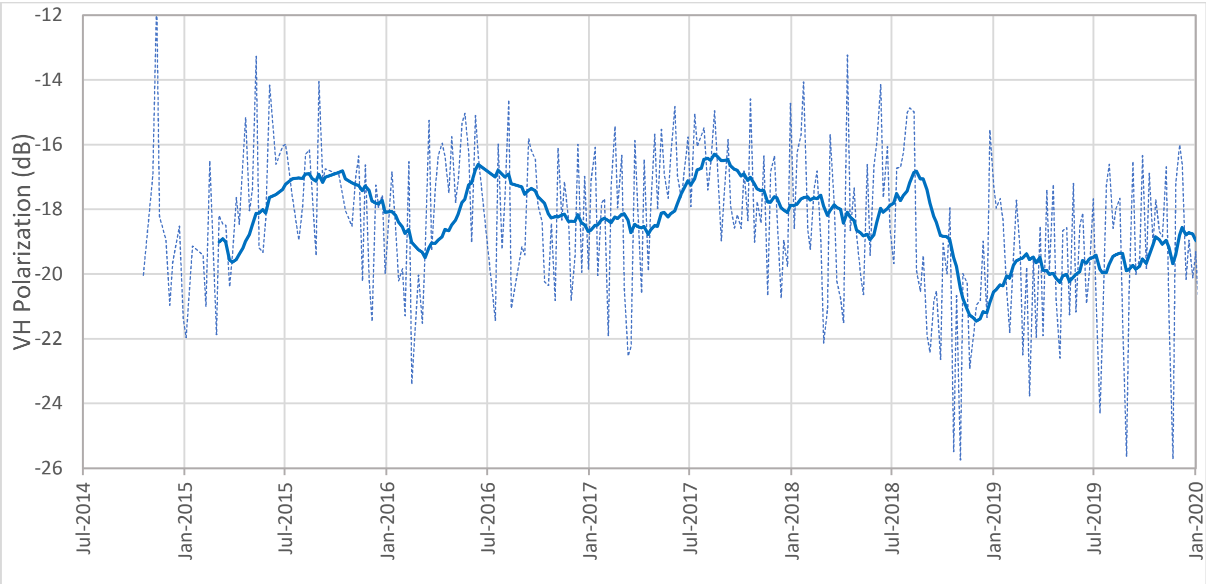

Figure 13: The temporal profile backscatter response of a known infestation process independent of study sample located in Rheinbrohl, towards west of Eifel NP. The canopy colour changed from normal green healthy to reddish infected spruce trees between 22 April 2018 and 24 April 2019, indicated by lack of seasonal pattern around September 2018 and thereafter.

3.6. The precipitation influence on the SAR temporal backscatter pattern

No relationship can be drawn between the SAR backscatter coefficient values of the spruce trees and the local precipitation events. Figure 14 illustrates the comparison of the backscatter response of both healthy and infected spruce trees with the corresponding precipitation data on the same time series scale. In Figure 14 (a), the green line indicates the backscatter response of healthy spruce trees, and blue bars indicate the precipitation events. Likewise, in Figure 14(b), the red line indicates the backscatter coefficients of the infected spruce trees and the blue bars indicate the subsequent precipitation events. Based on the visual interpretation of the graphs of Figure 14, there are no clear linkages visible between the backscatter signals and the precipitation events. Since there is no influence of rainfall on the backscatter coefficient, it was decided that there is no need to remove the expected outliers of SAR signals in the temporal profiles of the spruce trees.

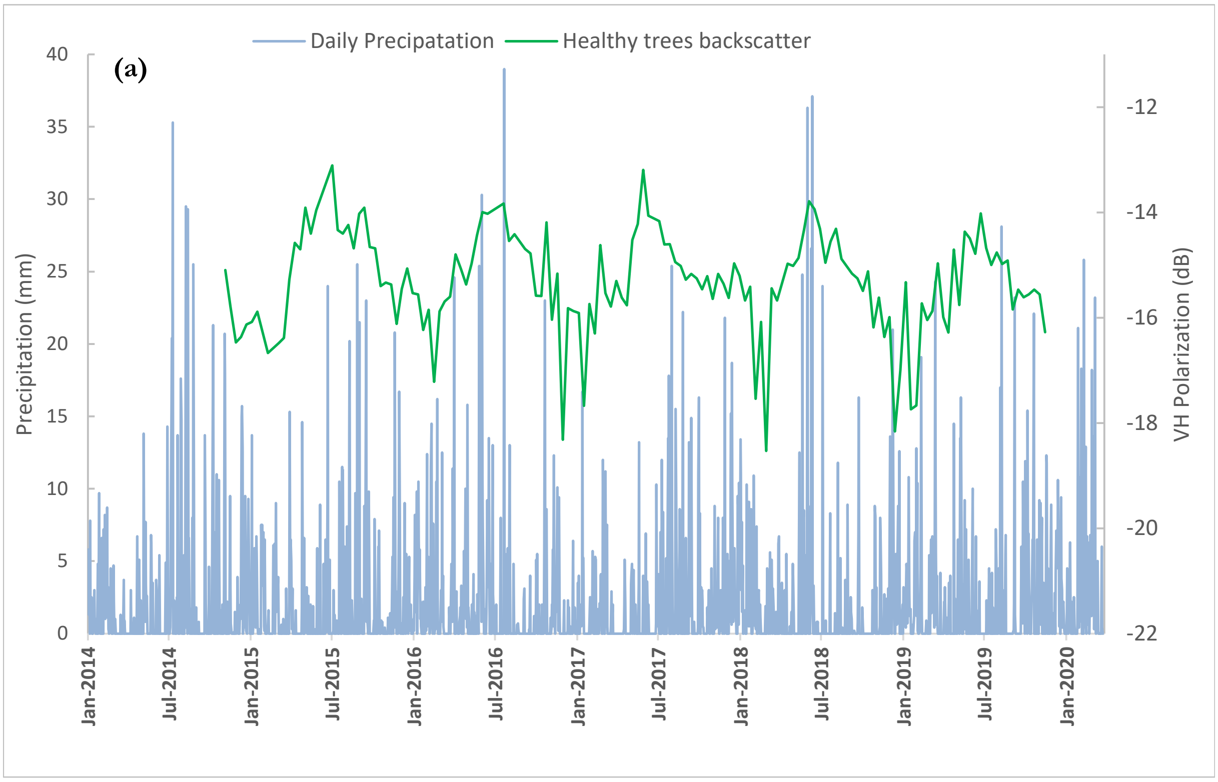

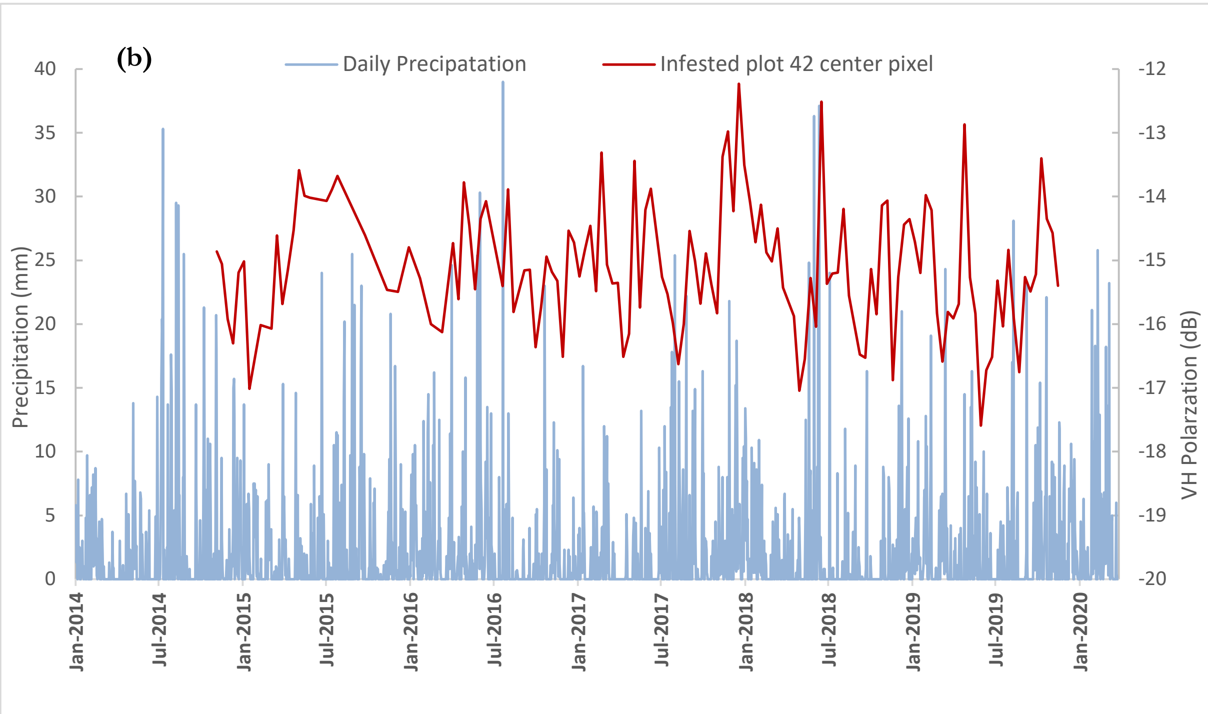

Figure 14(a & b): Daily precipitation observed at Mannebach/Eifel, Germany with, (a) VH polarization of healthy spruce tree sample, (b) VH polarization of infected spruce sample plot No. 42.

3.7. Sentinel-2 NDRE index-based temporal profile of healthy and infected spruce trees

The temporal profile based on Sentinel-2 Normalized Difference Red Edge (NDRE) index also shows the difference between the healthy and infected spruce trees. In the case of the NDRE temporal profile of an infected spruce tree, the NDRE index values range from 0 to up to 0.6 (Figure 15 a). Whereas the NDRE temporal profile of a healthy spruce tree indicates a higher range of NDRE index value between 0.4 to 0.7(Figure 15b). Comparing the trend between healthy and infected temporal profiles, there is decreased NDRE index values for the infected spruce trees around the year 2016 onwards. Such a change of the trend can be inferred as the infestation moment like the SAR backscatter temporal profile. However, it was found that only 23 timestamps of Sentinel-2 scenes were useful for building a temporal profile while rest were cloud contaminated for the study period from 2014 to 2019. Therefore, Sentinel-2 NDRE index-based temporal profile lacks a clear seasonal pattern for the healthy spruce trees.

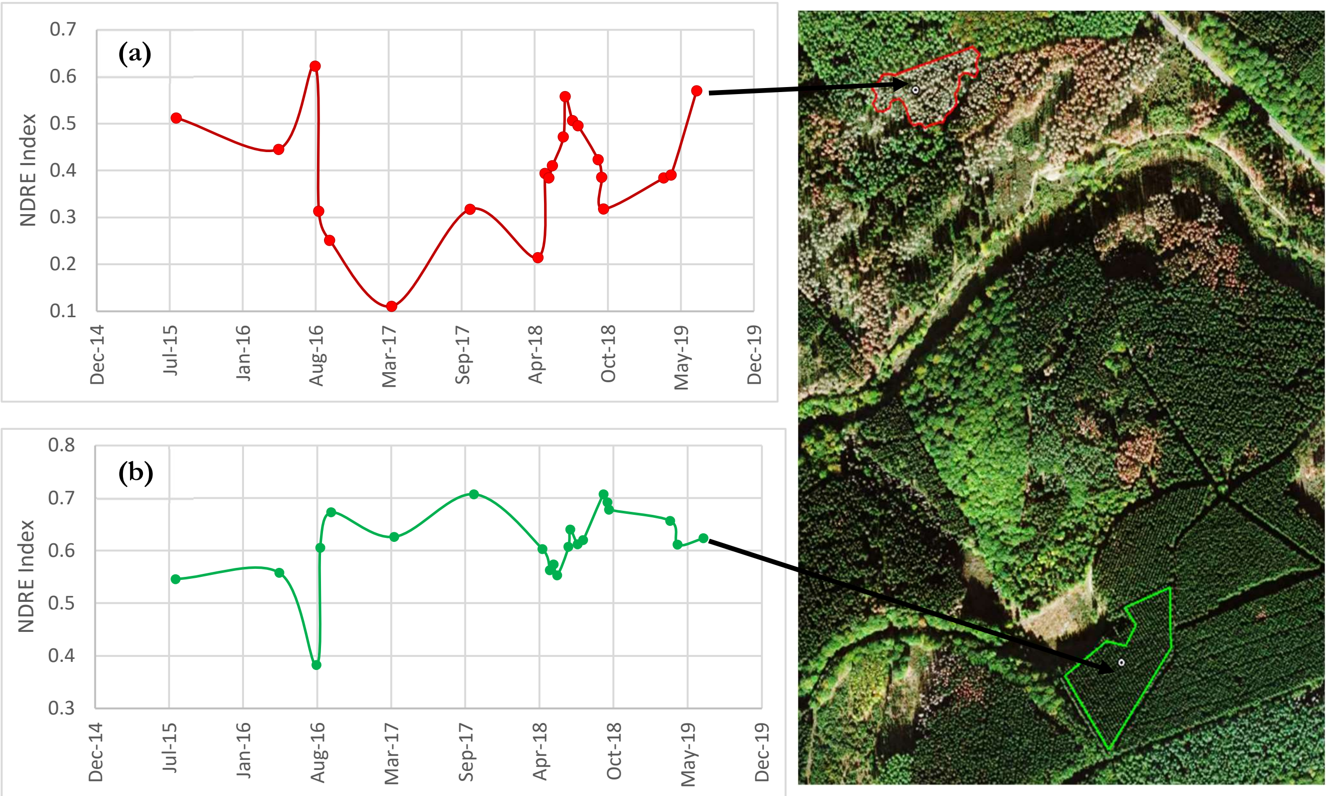

Figure 15 (a & b). Sentinel-2 NDRE Index temporal profile of infected and healthy spruce trees. (a) NDRE index temporal profile of the infected trees of the sample plot no. 30. (b) NDRE index temporal profile of the healthy spruce trees of the sampole plot no. 42.

4. DISCUSSION

Despite significant differences in the mean SAR backscatter response, a large overlap in their distribution may limit the distinction between healthy and infected trees based on a single time snapshot of a SAR image. However, the difference in the pattern of the SAR temporal profile between the healthy and infected spruce trees allows inferring the difference between the healthy and infected spruce trees.

4.1. The distribution and statistical difference between healthy and infected spruce trees

The distribution of Sentinel-1 SAR backscatter response of a healthy and infected spruce tree overlap substantially, limiting the potential of SAR backscatter to differentiate between them, despite a statistically significant difference with their mean backscatter response. Ranson et al. (2003) also found that JERS and Radarsat radar data showed the differences in terms of backscatter response between the insect-damaged and healthy coniferous trees. However, no previous studies explored the overlap in their backscatter distribution. The overlap of the SAR backscatter distribution could have impeded separability between the healthy and the infected spruce trees. Hence, the low separability could have resulted in poor image classification with the single date SAR based image of healthy and infected spruce trees. For example, Ranson et al. (2003) also reported a classification accuracy of 29% in a severe insect-damaged category and 46% in the moderately insect-damaged category.

The reasons for the major overlap in Sentinel-1 C-band SAR signal distribution between the healthy and infected spruce trees could be due to minimal change of their canopy structures. The canopy structure of the spruce tree remains unchanged since the bark beetle damages by interrupting water and the nutrient flow (Senf et al, 2017). So, the structure of the branches and twigs in the canopy remained the same after the infestation of the spruce trees. On the other hand, studies have found better classification accuracy with different sensors and different SAR bandwidths (Ortiz et al., 2013; Tanase et al., 2018). Thus, we may expect better separability results from other SAR sensors such as P-band and X-band SAR data. However, unlike Sentinel-1 SAR data, the cost of data acquisition associated with other SAR data may not be feasible for large scale monitoring of the bark beetle infestation of the spruce forests. Therefore, to leverage the rich temporal resolution of the Sentinel-1 SAR data rather than relying on a single snapshot of an image, the temporal profile was explored for differentiating between the healthy and infected spruce trees.

4.2. Adaptive Savitzky-Golay (ASAVGOL) Filter

Adaptive Savitzky-Golay (ASAVGOL) filter is expected to enhance the actual SAR backscatter response removing the noisy backscatter response of the annual profile. The enhanced annual profile after applying the ASAVGOL filter indicates the ability to filter out the noise and extract the actual signals of the healthy trees as expected. Hence, the improved annual profile has facilitated to better understand and differentiate between the healthy and infected spruce trees. The ASAVGOL method of filtering of time series pattern is consistent with what was followed by Dostálová et al, (2018) to enhance the weaker seasonal variations.

4.3. The annual temporal profile of the healthy and infected spruce trees

The time series profile pattern of a healthy spruce trees differs from the time series profile of an infected spruce trees based on their respective Sentinel-1 SAR signal response. The difference of the profile pattern indicates that there is a change of backscatter coefficients response after the bark beetle infestation of the spruce trees. The healthy tree shows a sinusoidal pattern whereas infected trees profile exhibits an irregular pattern. Both healthy and infected temporal profile patterns can be attributed to their respective physiological processes and natural phenomena of a plant life cycle.

These annual backscatter profiles of the healthy spruce trees follow the plant growing season of the annual growth cycles (Ahern et al, 1993; Hollaus & Vreugdenhil, 2019; Senf et al., 2017). The sinusoidal patterns show an ascending upward trend coinciding with the summer growing period and peaks in the months of June-July each year. Then it drops back down and dips low in the winter months of January-February each year. The high backscatter coefficients of the healthy spruce trees could be explained by the increase of the water content of the living foliages during the summer seasons. This is consistent with what studies have suggested that water content in the vegetative parts of the living tree leads to the higher dielectric constant which produces higher radar backscatter response (Attema & Ulaby, 1978; Öquist & Huner, 2003).

On the contrary to the annual profile of a healthy tree, the annual backscatter profiles of the infected spruce trees do not show any specific regular pattern after the infestation. The explanation for the moment of an infestation is relevant to the change in mean backscatter difference values after bark beetle infestation of the spruce trees. It was found that there was a mean backscatter coefficient difference of - 0.8 dB in VH polarization and -0.73 dB in VV polarization between the healthy and infected spruce trees (Table 1). The lowered backscatter coefficient values after the infestation moment can also be attributed to the reduced water content in the dying foliage of the beetle damaged tree canopy influencing the lower dielectric constant. Besides, the fading of the foliages of the infected spruce tree canopy might have exposed ground surface, contributing to erratic backscatter response as reported in other studies (Attema & Ulaby, 1978; Senf et al., 2017). The dead canopy of the infected trees likely allowed deeper penetration of Sentinel-1 C-band SAR signals, picking the backscatter signals of dry or wet soil, snow, or any other ground cover.

4.4. The moment of infestation: a transition from healthy to infected spruce tree captured by the temporal profile

The availability of high temporal resolution of the Sentinel-1 SAR data enables to obtain the moment of transition from healthy to the infected spruce tree using the temporal profile. The profile provides insight on the transitions where there is a change of the annual sinusoidal pattern into an unrecognizable form of a pattern on the time series profile. The temporal profiling technique shows a convincing indication that dense Sentinel-1 SAR time series or time dimension play a vital role to trace the moments of bark beetle impact on the physiological processes of the spruce trees. The ability of the temporal profile to reveal the moment of the bark beetle infestation is consistent with what was suggested by Hollaus & Vreugdenhil, (2019). Therefore, temporal profiling techniques could be deployed to understand and distinguish the moment of bark beetle damage at larger landscape level monitoring of the bark beetle infestations. Further, we can conclude that free and open availability of high temporal Sentinel-1 SAR data is applicable for monitoring bark beetle infestations.

Sentinel-1 SAR data has an advantage over Sentinel-2 optical data for monitoring bark beetle infestation. Although studies (Abdullah et al., 2018, 2019a) have found that Sentinel-2 optical data could detect early stage of bark beetle infestation, however, optical data acquisition is hampered by could contamination. For instance, only 23timestamps of Sentinel-2 optical images could be collected from the year 2014 to 2019 for this study period. While, the duration of bark beetle infestation of the spruce trees, happens to occur within a short span of a few months, it impairs monitoring capability with less temporal coverage. Consequently, Sentinel-1 SAR data independent of cloud contamination may be far more effective for monitoring the bark beetle infestation of spruce forests.

4.5. Limitations

This study lacked the field-based samples for both healthy and infected spruce trees. Samples were collected using the high resolution google earth images the visual interpretation. Thus, the samples for both healthy and infected are based on the critical assumption that visual interpretation truly represents actual spruce trees of both healthy and infected sample category.

Since there was no field-based sample data, the relationship between the moment of infestation indicated by the temporal profile and the different stages of bark beetle infestation could not be investigated. Hollaus & Vreugdenhil, (2019) also mentioned about lack of available infected samples data to analyze differences between healthy and infected spruce backscatter using time series profile. The possible reason for the lack of field-based data is due to the huge requirements of field monitoring resources and difficulty in identifying the different stages of bark beetle infestation (Hlásny et al., 2019; Wulder et al., 2005). To understand at what stage of bark beetle infestation could be explained by the temporal profile, a study using field-based samples is necessary.

The findings may be applicable to differentiate healthy and infected trees where there is pure spruce stand but not in a forest area with the spruce mixed with other tree species. Since the study was located within Eifel National Park, the study sample sites mostly contained pure spruce stands. In mixed forests, the SAR signal of the healthy spruce tree can mix with the other tree species and the SAR signal of infected spruce trees also is combined with other tree species. Such a mixed SAR backscatter response is likely to cause a less clear separability of healthy and infected trees.

The pattern of the temporal profile was not explicitly apparent to show the difference between the healthy and infected category for a few of the sample plots. Speculation arises for the sensitivity of SAR backscatter response to local landscape environmental conditions. For this purpose, to find out the effect of precipitation to backscatter response, local in situ precipitation data were simultaneously plotted alongside the time series profile. Coherently with the previous studies (Rüetschi et al., 2019), no influence of precipitation was observed on the SAR backscatter response.

The temporal profiling method to differentiate between healthy and infected spruce trees may not be suited for some purpose. For example, since not every deviation from the expected seasonal pattern is pointing at an infestation, this method may not work well to alert forest managers to react immediately. With the Sentinel-1 temporal profiling method, the moment of bark beetle damage could be pointed but it is not clear say at what stage of bark beetle infestation.

4.6. Possible application

The ability of the SAR profiling technique to identify bark beetle affected trees can be applied to guide forest managers to mitigate further spreading onto other healthy trees. It would serve as the cost-effective remote sensing technique required by forest managers and private forest owners to consistently monitor the bark beetle outbreaks in a spruce forests (Hlásny et al., 2019; Kolb et al., 2016; Křivan et al., 2016; Pellizzoni, 2011). According to Hlásny et al. (2019), the most strategic forest management intervention to mitigate the widespread of bark beetle infestation is identifying bark beetle outbreaks and removing infected trees which are also known as sanitation operations. Therefore, the temporal profiling technique of differentiating between the healthy and infected spruce trees would guide the forest manager by identifying the bark beetle outbreak site for a timely sanitation operation. It would be efficient and cost-effective than the conventional field surveys (Fettig & Hilszczański, 2015) since Sentinel-1 SAR is openly available globally. This is in line with Hollaus & Vreugdenhil, (2019) who pointed out that high temporal resolution of the Sentinel-1 C-band has potential for monitoring the bark beetle infestations.

Relevant agencies can apply SAR temporal profiling techniques to identify the bark beetle infestation that helps make informed decisions for certifying sustainable forest management and compensation measures for forest owners affected by the bark beetle outbreak. For example, the German government had to allocate about eight million euros for 2019 and 2020 as relief support to the forest owners in reclaiming and salvaging bark beetle affected forests (Teller Report, 2019). The SAR temporal profiling method could be applied for screening the compensation of bark beetle damage claims of the local forest owners (Hlásny et al., 2019). Besides, this method can also be applied to examine the bark beetle mitigation measure implemented by forest managers for certification of sustainable forest management to be considered as sustainable status.

4.7. Conclusion

The SAR temporal profiling technique would be relevant to provide a solution for the requirement of cost-efficient remote sensing technology for monitoring bark beetle infestation (Hlásny et al., 2019). This method is also expected to serve as a solution for the requirement of a remote sensing method to improve bark beetle detection and mapping which was a priority research problem identified by the ecologists, land managers and social scientists across North America and Europe (Morris et al., 2017). This method is considered to be cost-efficient as the Sentinel-1 SAR data is freely and openly available. Further, it may substitute or at least compliment the current methods of identifying the bark beetle infestation, replacing the physically challenging and resource-intensive exercises (Fettig & Hilszczański, 2015).

The SAR temporal profiling method is suitable than a single time snapshot Sentinel-1 SAR image to differentiate between healthy and bark beetle infected spruce trees. Despite a statistically significant difference between the means of Sentinel-1 SAR backscatter coefficients coming from healthy and a bark beetle infected spruce tree, there was a large overlap in their distribution that could hinder differentiation of their SAR signals. Hence, a workable method to use a single time snapshot Sentinel-1 image is unlikely to distinguish between the healthy and infected spruce trees. Sentinel-2 optical bands would be better alternatives for a single time snapshot image classification as studied by (Abdullah et al., 2019a; Yang, 2019). However, temporal profiling techniques using Sentinel-1 SAR data was found to be a useful method to differentiate between healthy and infected spruce trees which were not possible with Sentinel-2 image.

The temporal profiling technique exploits the time dimension to churn out insightful information for remote sensing application. For example, Sentinel-1 SAR images were found suitable to understand the impact of the moment of bark beetle infestation on spruce trees by temporal profiling technique. The availability of high temporal Sentinel-1 SAR permits to illustrate the difference between the annual phenological activity of living spruce trees and the dying spruce trees infected by the bark beetles. Furthermore, the Adaptive Savitzky-Golay filter improves the seasonal pattern information content of the time series backscatter response by removing noise and enhancing the readability of the pattern explicitly. The profiling technique to reveal the moment of bark beetle impact on the spruce trees was validated with the independent data. Therefore, we can conclude that Sentinel-1 SAR backscatter data allows exploiting the time dimension with temporal profiling methods to distinguish between the healthy and infected spruce trees for monitoring bark beetle infestation over the larger landscape.

Sentinel-1 SAR images were found better than Sentinel-2 optical images in the temporal profiling method to understand the differences between the healthy and infected spruce trees. Since Sentinel-1 SAR data is not hampered by cloud contamination, it has an advantage over Sentinel-2 optical that allowed with numerous uninterrupted time-series data. On the other hand, Sentinel-2 based NDRE time series index was not able to form an annual pattern due to limited cloud-free observations. Thus, Sentinel-2 might be of limited use for monitoring technique of bark beetle infestation of spruce forest in an area that remains mostly cloudy throughout the year. However, Sentinel-2 optical has advantages of better separability and detecting early-stage of bark beetle infestation as studied by Abdullah et al., (2019a).

Sentinel-1 SAR temporal profiling techniques to find out the moment of bark beetle impact on the spruce trees would be useful for forest management and sustainable certification of forest management. It would provide information to guide forest managers and forest owners on the infected area for controlling further spreading into the entire forests (Carter et al., 1998; Chen & Meentemeyer, 2016). Sustainable certification institutes can use this method to assess and validate the extent of the bark beetle damage areas cost-effectively. For example, this method could be used by the relevant agencies that require evidence of the bark beetle damage to regulate the compensation of pests and diseases to forest owners (Hlásny et al., 2019).

Further investigation is necessary to understand at what stage of bark beetle infestation can be described by the SAR temporal profile using field-based samples at each stage of the infestation processes. The future study using field-based sample data is expected to establish the relationship between the moment of infestation captured by the temporal profile and the different stages of bark beetle infestation. The relationship between the moment of infestation and stages of bark infestation would be useful for monitoring and detection of bark beetle infestation ina spruce forests.

LIST OF REFERENCES

Abdullah, H., Darvishzadeh, R., Skidmore, A. K., Groen, T. A., & Heurich, M. (2018). European spruce bark beetle (Ips typographus, L.) green attack affects foliar reflectance and biochemical properties. *International Journal of Applied Earth Observation and Geoinformation*, *64*, 199–209. https://doi.org/10.1016/j.jag.2017.09.009

Abdullah, H., Skidmore, A. K., Darvishzadeh, R., & Heurich, M. (2019a). Sentinel-2 accurately maps green-attack stage of European spruce bark beetle (Ips typographus, L.) compared with Landsat-8. *Remote Sensing in Ecology and Conservation*, *5*(1), 87–106. https://doi.org/10.1002/rse2.93

Abdullah, H., Skidmore, A. K., Darvishzadeh, R., & Heurich, M. (2019b). Timing of red-edge and shortwave infrared reflectance critical for early stress detection induced by bark beetle (Ips typographus, L.) attack. *International Journal of Applied Earth Observation and Geoinformation*, *82*, 101900. https://doi.org/10.1016/j.jag.2019.101900

Ahern, F. J., Leckie, D. J., & Drieman, J. A. (1993). Seasonal Changes in Relative C-Band Backscatter of Northern Forest Cover Types. *IEEE Transactions on Geoscience and Remote Sensing*, *31*(3), 668–680. https://doi.org/10.1109/36.225533

Alamy Limited. (2019). North Rhine-Westphalia, Köln: A cone hangs from a spruce. Retrieved September 20, 2019, from Almy website: https://www.alamy.com/18-april-2019-north-rhine-westphalia-kln-a-cone-hangs-from-a-spruce-storms-drought-bark-beetles-2018-was-a-stressful-year-for-the-forest-in-germany-on-the-day-of-the-tree-april-25th-there-are-signs-that-this-will-continue-in-regions-

ASF. (n.d.). ASF Data Search. Retrieved February 20, 2020, from https://search.asf.alaska.edu/#/

Attema, E. P. W., & Ulaby, F. T. (1978). Vegetation modeled as a water cloud. *Radio Science*, *13*(2), 357–364. https://doi.org/10.1029/RS013i002p00357

Bentz, B. J., Jönsson, A. M., Schroeder, M., Weed, A., Wilcke, R. A. I., & Larsson, K. (2019). Ips typographus and Dendroctonus ponderosae Models Project Thermal Suitability for Intra- and Inter-Continental Establishment in a Changing Climate. *Frontiers in Forests and Global Change*, *2*. https://doi.org/10.3389/ffgc.2019.00001

Biedermann, P. H. W., Müller, J., Grégoire, J. C., Gruppe, A., Hagge, J., Hammerbacher, A., … Bässler, C. (2019). Bark Beetle Population Dynamics in the Anthropocene: Challenges and Solutions. *Trends in Ecology and Evolution*. https://doi.org/10.1016/j.tree.2019.06.002

Boone, C. K., Aukema, B. H., Bohlmann, J., Carroll, A. L., & Raffa, K. F. (2011). Efficacy of tree defense physiology varies with bark beetle population density: A basis for positive feedback in eruptive species. *Canadian Journal of Forest Research*, *41*(6), 1174–1188. https://doi.org/10.1139/x11-041

Boyd, I. L., Freer-Smith, P. H., Gilligan, C. A., & Godfray, H. C. J. (2013). The consequence of tree pests and diseases for ecosystem services. *Science*, Vol. 342. https://doi.org/10.1126/science.1235773

Bright, B. C., Hicke, J. A., & Meddens, A. J. H. (2013). Effects of bark beetle-caused tree mortality on biogeochemical and biogeophysical MODIS products. *Journal of Geophysical Research: Biogeosciences*, *118*(3), 974–982. https://doi.org/10.1002/jgrg.20078

Cailleret, M., Nourtier, M., Amm, A., Durand-Gillmann, M., & Davi, H. (2014). Drought-induced decline and mortality of silver fir differ among three sites in Southern France. *Annals of Forest Science*, *71*(6), 643–657. https://doi.org/10.1007/s13595-013-0265-0

Carter, G. A., Seal, M. R., & Haley, T. (1998). Airborne detection of southern pine beetle damage using key spectral bands. *Canadian Journal of Forest Research*, *28*(7), 1040–1045.

Chen, G., & Meentemeyer, R. K. (2016). Remote Sensing of Forest Damage by Diseases and Insects. In *Remote Sensing for Sustainability* (pp. 145–162). https://doi.org/10.1201/9781315371931-9

Chinellato, F., Faccoli, M., Marini, L., & Battisti, A. (2014). Distribution of Norway spruce bark and wood-boring beetles along Alpine elevational gradients. *Agricultural and Forest Entomology*, *16*(2), 111–118. https://doi.org/10.1111/afe.12040

Christiansen, E., & Bakke, A. (1988). The Spruce Bark Beetle of Eurasia. In *Dynamics of Forest Insect Populations* (pp. 479–503). https://doi.org/10.1007/978-1-4899-0789-9_23

Coops, N. C., Johnson, M., Wulder, M. A., & White, J. C. (2006). Assessment of QuickBird high spatial resolution imagery to detect red attack damage due to mountain pine beetle infestation. *Remote Sensing of Environment*, *103*(1), 67–80. https://doi.org/10.1016/j.rse.2006.03.012

Darvishzadeh, R., Skidmore, A., Abdullah, H., Cherenet, E., Ali, A., Wang, T., … Paganini, M. (2019). Mapping leaf chlorophyll content from Sentinel-2 and RapidEye data in spruce stands using the invertible forest reflectance model. *International Journal of Applied Earth Observation and Geoinformation*, *79*, 58–70. https://doi.org/10.1016/j.jag.2019.03.003

Deutsche Welle. (2019). Storms and drought destroy thousands of acres of German forests | News | DW | 26.04.2019. Retrieved September 7, 2019, from https://www.dw.com/en/storms-and-drought-destroy-thousands-of-acres-of-german-forests/a-48493443

Dostálová, A., Wagner, W., Milenković, M., & Hollaus, M. (2018). Annual seasonality in Sentinel-1 signal for forest mapping and forest type classification. *International Journal of Remote Sensing*, *39*(21), 7738–7760. https://doi.org/10.1080/01431161.2018.1479788

Egan, J. M., Sloughter, J. M. L., Cardoso, T., Trainor, P., Wu, K., Safford, H., & Fournier, D. (2016). Multi-temporal ecological analysis of Jeffrey pine beetle outbreak dynamics within the Lake Tahoe Basin. *Population Ecology*, *58*(3), 441–462. https://doi.org/10.1007/s10144-016-0545-2

ESA. (2019). Data products / Sentinel-1 / Copernicus / Observing the Earth / Our Activities / ESA. Retrieved October 3, 2019, from https://www.esa.int/Our_Activities/Observing_the_Earth/Copernicus/Sentinel-1/Data_products

Fassnacht, F. E., Latifi, H., Ghosh, A., Joshi, P. K., & Koch, B. (2014). Assessing the potential of hyperspectral imagery to map bark beetle-induced tree mortality. *Remote Sensing of Environment*, *140*, 533–548. https://doi.org/10.1016/j.rse.2013.09.014

Fettig, C. J., & Hilszczański, J. (2015). Management Strategies for Bark Beetles in Conifer Forests. In *Bark Beetles: Biology and Ecology of Native and Invasive Species* (pp. 555–584). https://doi.org/10.1016/B978-0-12-417156-5.00014-9

Frampton, W. J., Dash, J., Watmough, G., & Milton, E. J. (2013). Evaluating the capabilities of Sentinel-2 for quantitative estimation of biophysical variables in vegetation. *ISPRS Journal of Photogrammetry and Remote Sensing*, *82*, 83–92. https://doi.org/10.1016/j.isprsjprs.2013.04.007

GFOI. (2018). A layman's interpretation guide to L-band and C-band synthetic aperture radar data. In *Committee on Erath Observation Satellites* (Vol. 2).

Gorelick, N., Hancher, M., Dixon, M., Ilyushchenko, S., Thau, D., & Moore, R. (2017). Google Earth Engine: Planetary-scale geospatial analysis for everyone. *Remote Sensing of Environment*, *202*, 18–27. https://doi.org/10.1016/j.rse.2017.06.031

Hais, M., Wild, J., Berec, L., Brůna, J., Kennedy, R., Braaten, J., & Brož, Z. (2016). Landsat imagery spectral trajectories-important variables for spatially predicting the risks of bark beetle disturbance. *Remote Sensing*, *8*(8). https://doi.org/10.3390/rs8080687

Heine, P., Hausen, J., Ottermanns, R., Schäffer, A., & Roß-Nickoll, M. (2019). Forest conversion from Norway spruce to European beech increases species richness and functional structure of aboveground macrofungal communities. *Forest Ecology and Management*, *432*, 522–533. https://doi.org/10.1016/j.foreco.2018.09.012

Hlásny, T., Krokene, P., Liebhold, A., Montagné-Huck, C., Müller, J., Qin, H., … Svoboda, M. (2019). *Living with bark beetles: impacts, outlook and management options: From Science to Policy 8*.

Hollaus, M., & Vreugdenhil, M. (2019, December 1). Radar Satellite Imagery for Detecting Bark Beetle Outbreaks in Forests. *Current Forestry Reports*, Vol. 5, pp. 240–250. https://doi.org/10.1007/s40725-019-00098-z

IPCC. (2018). Summary for Policymakers. In V. Masson-Delmotte, P. Zhai, H.-O. Pörtner, D. Roberts, J. Skea, P. R. Shukla, … T. Waterfield (Eds.), *Global Warming of 1.5°C. An IPCC Special Report on the impacts of global warming of 1.5°C above pre-industrial levels and related global greenhouse gas emission pathways, in the context of strengthening the global response to the threat of climate change* (p. 32). Retrieved from https://www.ipcc.ch/site/assets/uploads/sites/2/2018/07/SR15_SPM_version_stand_alone_LR.pdf

Kautz, M., Schopf, R., & Imron, M. A. (2014). Individual traits as drivers of spatial dispersal and infestation patterns in a host-bark beetle system. *Ecological Modelling*, *273*, 264–276. https://doi.org/10.1016/j.ecolmodel.2013.11.022

Kolb, T. E., Fettig, C. J., Ayres, M. P., Bentz, B. J., Hicke, J. A., Mathiasen, R., … Weed, A. S. (2016). Observed and anticipated impacts of drought on forest insects and diseases in the United States. *Forest Ecology and Management*, *380*, 321–334. https://doi.org/10.1016/j.foreco.2016.04.051

Křivan, V., Lewis, M., Bentz, B. J., Bewick, S., Lenhart, S. M., & Liebhold, A. (2016). A dynamical model for bark beetle outbreaks. *Journal of Theoretical Biology*, *407*, 25–37. https://doi.org/10.1016/j.jtbi.2016.07.009

Langstrom, B., Lindelöw, Å., Schroeder, M., Björklund, N., & Öhrn, P. (2009). *The spruce bark beetle outbreak in Sweden following the January-storms in 2005 and 2007*.

Latifi, H., Fassnacht, F. E., Schumann, B., & Dech, S. (2014). Object-based extraction of bark beetle (Ips typographus L.) infestations using multi-date LANDSAT and SPOT satellite imagery. *Progress in Physical Geography*, *38*(6), 755–785. https://doi.org/10.1177/0309133314550670

Laurin, G. V., Balling, J., Corona, P., Mattioli, W., Papale, D., Puletti, N., … Urban, M. (2018). Above-ground biomass prediction by Sentinel-1 multitemporal data in central Italy with integration of ALOS2 and Sentinel-2 data. *Journal of Applied Remote Sensing*, *12*(01), 1. https://doi.org/10.1117/1.JRS.12.016008

Meddens, A. J. H., Hicke, J. A., Vierling, L. A., & Hudak, A. T. (2013). Evaluating methods to detect bark beetle-caused tree mortality using single-date and multi-date Landsat imagery. *Remote Sensing of Environment*, *132*, 49–58. https://doi.org/10.1016/j.rse.2013.01.002

Morris, J. L., Cottrell, S., Fettig, C. J., Hansen, W. D., Sherriff, R. L., Carter, V. A., … Seybold, S. J. (2017, June 1). Managing bark beetle impacts on ecosystems and society: priority questions to motivate future research. *Journal of Applied Ecology*, Vol. 54, pp. 750–760. https://doi.org/10.1111/1365-2664.12782

Müller, M. (2011). How natural disturbance triggers political conflict: Bark beetles and the meaning of landscape in the Bavarian Forest. *Global Environmental Change*, *21*(3), 935–946. https://doi.org/10.1016/j.gloenvcha.2011.05.004

Niemann, K. O., & Visintini, F. (2005). Assessment of potential for remote sensing detection of bark beetle-infested areas during green attack : a literature review Assessment of potential for remote sensing detection of bark beetle-infested areas during green attack : a literature review. In *Natural Resources Canada, Canadian Forest Service*. https://doi.org/10.1017/CBO9781107415324.004

Öhrn, P., Långström, B., Lindelöw, Å., & Björklund, N. (2014). Seasonal flight patterns of Ips typographus in southern Sweden and thermal sums required for emergence. *Agricultural and Forest Entomology*, *16*(2), 147–157. https://doi.org/10.1111/afe.12044

Öquist, G., & Huner, N. P. A. (2003). P HOTOSYNTHESIS OF O VERWINTERING E VERGREEN P LANTS. *Annual Review of Plant Biology*, *54*(1), 329–355. https://doi.org/10.1146/annurev.arplant.54.072402.115741

Ortiz, S. M., Breidenbach, J., & Kändler, G. (2013). Early detection of bark beetle green attack using terraSAR-X and rapideye data. *Remote Sensing*, *5*(4), 1912–1931. https://doi.org/10.3390/rs5041912

Overbeck, M., & Schmidt, M. (2012). Modelling infestation risk of Norway spruce by Ips typographus (L.) in the Lower Saxon Harz Mountains (Germany). *Forest Ecology and Management*, *266*, 115–125. https://doi.org/10.1016/j.foreco.2011.11.011

Pellizzoni, L. (2011). Governing through disorder: Neoliberal environmental governance and social theory. *Global Environmental Change*, *21*(3), 795–803. https://doi.org/10.1016/j.gloenvcha.2011.03.014

Pureswaran, D. S., Roques, A., & Battisti, A. (2018). Forest insects and climate change. *Current Forestry Reports*, *4*(2), 35–50. https://doi.org/10.1007/s40725-018-0075-6

QGIS Development Team. (2020). *QGIS Geographic Information System. Open Source Geospatial Foundation Project.*

Ranghetti, L., & Busetto, L. (2019). *sen2r: Find, Download and Process Sentinel-2 Data*. https://doi.org/10.5281/zenodo.1240384

Ranson, K. J., Kovacs, K., Sun, G., & Kharuk, V. I. (2003). Disturbance recognition in the boreal forest using radar and Landsat-7. *Canadian Journal of Remote Sensing*, *29*(2), 271–285. https://doi.org/10.5589/m02-096

Rüetschi, M., Schaepman, M. E., & Small, D. (2017). Using Multitemporal Sentinel-1 C-band Backscatter to Monitor Phenology and Classify Deciduous and Coniferous Forests in Northern Switzerland. *Remote Sensing*, *10*(2), 55. https://doi.org/10.3390/rs10010055

Rüetschi, M., Small, D., & Waser, L. T. (2019). Rapid detection of windthrows using Sentinel-1 C-band SAR data. *Remote Sensing*, *11*(2), 1–23. https://doi.org/10.3390/rs11020115

Ryan, M. G., Sapes, G., Sala, A., & Hood, S. M. (2015, February 1). Tree physiology and bark beetles. *New Phytologist*, Vol. 205, pp. 955–957. https://doi.org/10.1111/nph.13256

Saatchi, S., Asefi-Najafabady, S., Malhi, Y., Aragão, L. E. O. C., Anderson, L. O., Myneni, R. B., & Nemani, R. (2013). Persistent effects of a severe drought on Amazonian forest canopy. *Proceedings of the National Academy of Sciences of the United States of America*, *110*(2), 565–570. https://doi.org/10.1073/pnas.1204651110

Schmiedel, I., Goedecke, F., & Bergmeier, E. (2019). Plant communities of the Eifel National Park (Germany)-An assessment based on the first Permanent Plot Inventory. *Tuexenia*, *39*, 41–74. https://doi.org/10.14471/2019.39.015

Scott, J. T., Siccama, T. G., Johnson, A. H., & Breisch, A. R. (1984). Decline of Red Spruce in the Adirondacks, New York. *Bulletin of the Torrey Botanical Club*, *111*(4), 438. https://doi.org/10.2307/2995893

Senf, C., Seidl, R., & Hostert, P. (2017, August 1). Remote sensing of forest insect disturbances: Current state and future directions. *International Journal of Applied Earth Observation and Geoinformation*, Vol. 60, pp. 49–60. https://doi.org/10.1016/j.jag.2017.04.004

Siccama, T. G., Bliss, M., & Vogelmann, H. W. (1982). Decline of Red Spruce in the Green Mountains of Vermont. *Bulletin of the Torrey Botanical Club*, *109*(2), 162. https://doi.org/10.2307/2996256

Solheim, H. (1992). The early stages of fungal invasion in Norway spruce infested by the bark beetle Ips typographus. *Canadian Journal of Botany*, *70*(1), 1–5. https://doi.org/10.1139/b92-001

Tanase, M. A., Aponte, C., Mermoz, S., Bouvet, A., Le Toan, T., & Heurich, M. (2018). Detection of windthrows and insect outbreaks by L-band SAR: A case study in the Bavarian Forest National Park. *Remote Sensing of Environment*, *209*, 700–711. https://doi.org/10.1016/j.rse.2018.03.009

Teller Report. (2019). Forest: In Saxony threatens largest bark beetle plague since the Second World War - Teller Report. Retrieved September 7, 2019, from https://www.tellerreport.com/tech/--forest--in-saxony-threatens-largest-bark-beetle-plague-since-the-second-world-war-.Hy2QbJNwE.html

Wermelinger, B. (2004). Ecology and management of the spruce bark beetle Ips typographus - A review of recent research. *Forest Ecology and Management*, *202*(1–3), 67–82. https://doi.org/10.1016/j.foreco.2004.07.018

White, J. C., Coops, N. C., Hilker, T., Wulder, M. A., & Carroll, A. L. (2007). Detecting mountain pine beetle red attack damage with EO-1 hyperion moisture indices. *International Journal of Remote Sensing*, *28*(10), 2111–2121. https://doi.org/10.1080/01431160600944028

Wulder, M. A., Dymond, C. C., & White, J. (2005). *Remote sensing in the survey of mountain pine beetle impacts : Review and recommendations*. Canada.

XUE, J., YU, L., LIN, Q., LIU, G., HUANG, H., XUE, J., … HUANG, H. (2018). Using Sentinel-1 multi-temporal InSAR data to monitor the damage degree of shoot beetle in Yunnan pine forest. *Remote Sensing for Land & Resources*, *30*(4), 108–114. https://doi.org/10.6046/GTZYYG.2018.04.17

Yang, S. (2019). *Detecting bark beetle damage with Sentinel-2 multi-temporal data in Sweden*. Lund University.

APPENDICES

Appendix A. Using Alaska Satellite Facility or Vertex DAAC data search for obtaining Sentinel-1 SAR data

1. Use ASF web interface for filtering, selecting and setting downloading criteria (ASF).
2. Datasets: Sentinel 1 A
3. Draw box encompassing Eifel National Park and the study area polygon marked shown by yellow bounding box
4. In Additional filter:
5. File: L1Detected High-Res Dual-Pol (GRD-HD)
6. Beam mode: IW
7. Polarization: VV+VH
8. Direction: Ascending
9. SubType: SA
10. Path and Frame Filters: Start Path 88
11. Downloaded using python scripts and run the python script from the folder where the scripts have been saved and the data are downloaded into the same folder.
12. Organize and arrange downloaded sentinel 1 imageries: directory label S1A_P88_ACD
13. Separate yearly basis directory in order to ease the batch processing: 2014 to 2019

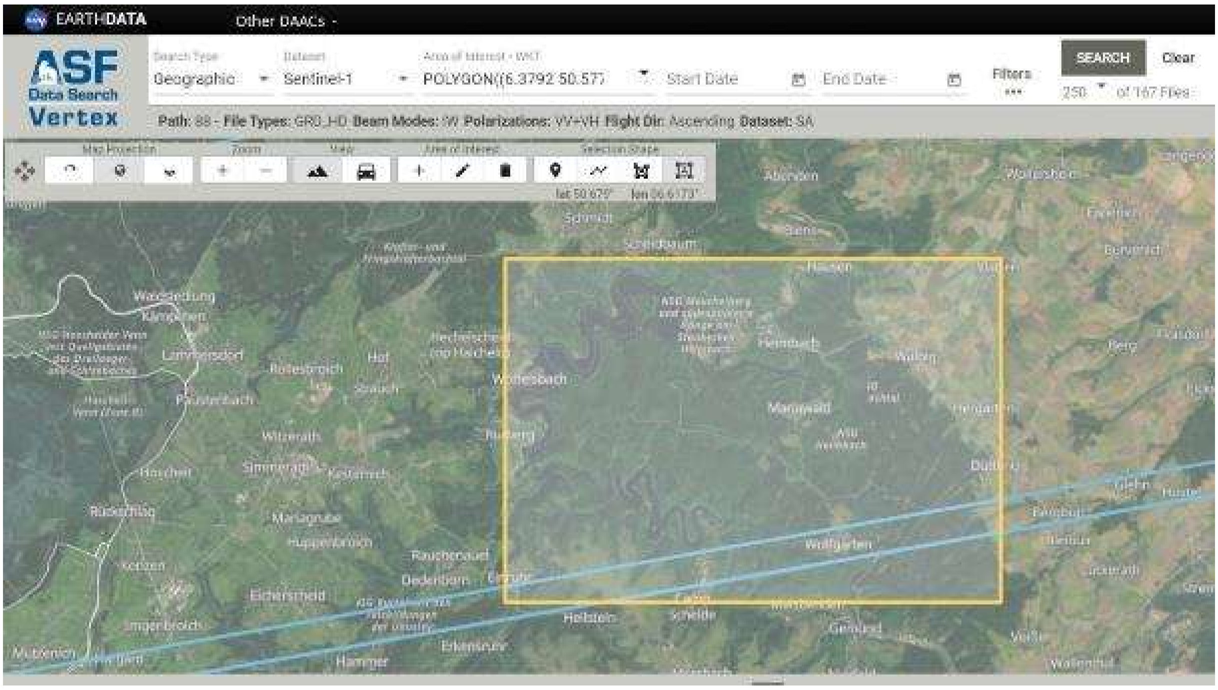

Appendix B. Using QGIS to generate sample points inside the infected and healthy sample polygons.

1. Convert the sample polygons digitized in Google Earth from KMZ format to shapefile format using any GIS software.
2. Use QGIS, Vector, research tools and regular points to generated distributed points of 20 m X 20 m across the healthy sample polygons.
3. Distribution of sample points for healthy samples was considered at a larger distance than infected sample since infected sample areas were comparatively smaller and not abundant as healthy samples.
4. Similarly, use QGIS, Vector, research tools and regular points to generated distributed points of 10 m X 10 m across the infected sample polygons.
5. Use QGIS, processing tools, point on the surface to generate the centre point of infected and healthy sample polygons to be used for extracting time-series SAR signals.
6. Centre point of the polygon was considered for time series analysis of SAR signal to avoid influence border pixels other than spruce trees.

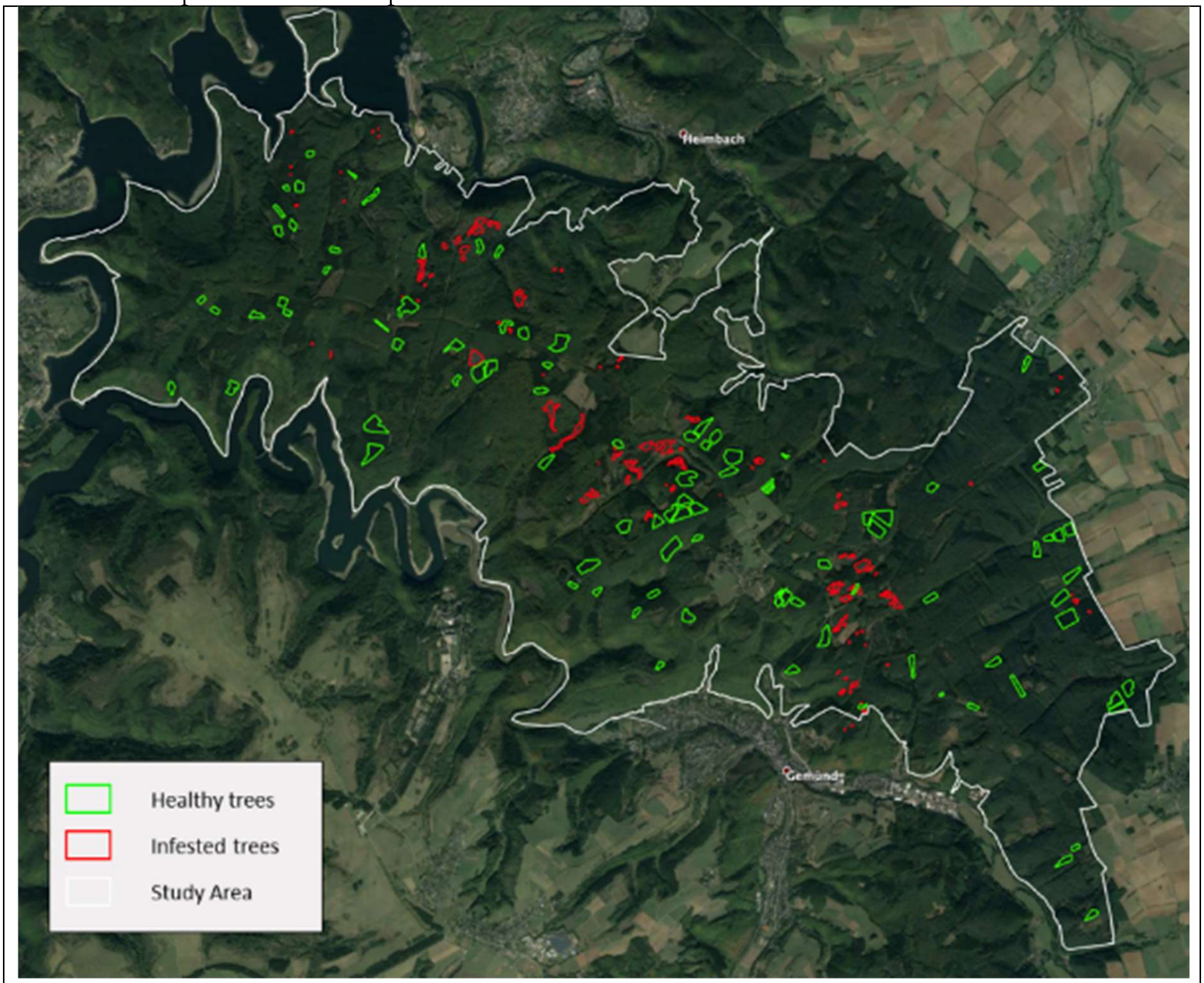

Appendix C. SAR Band math computation in SNAP

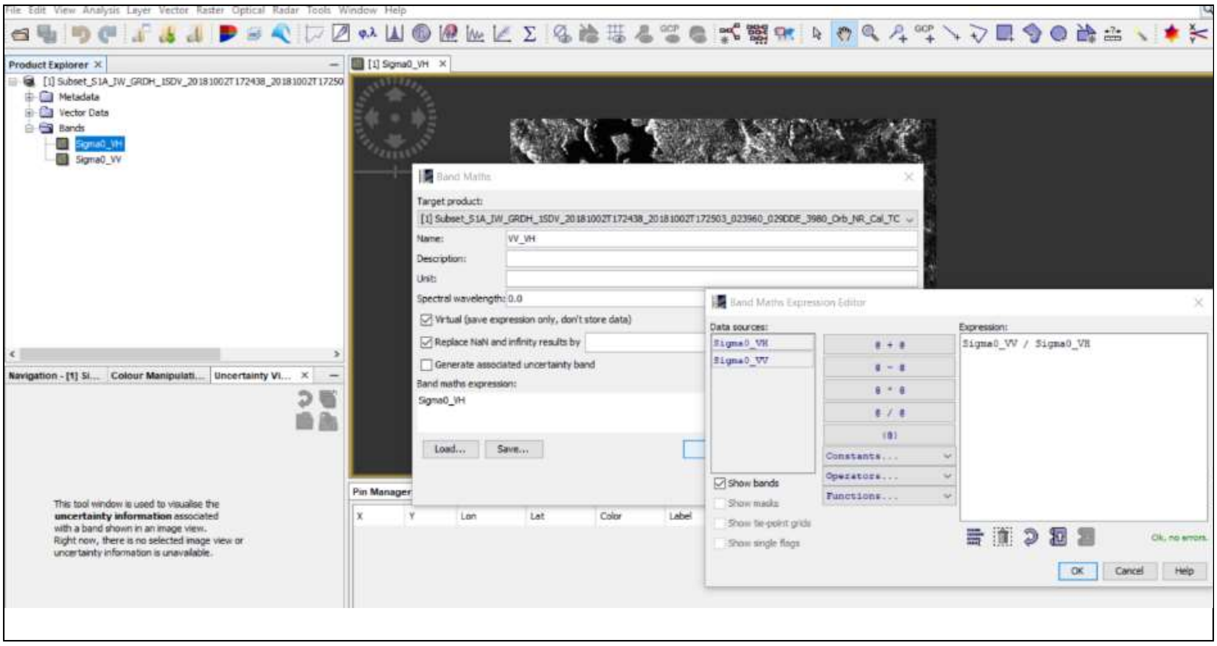

Screenshot of how to compute ratio polarization using band math function in SANP platform.

Appendix D. Extracting SAR signal using sample points for analysis

1. Load the SAR scene into the SNAP platform.
2. Go to Raster>Export>Extract pixel values.
3. Click on the + sign to add all the time series SAR images.
4. In the Input/Output tab checkmark the option to select all to add all the images for extracting their pixel values or SAR signals.
5. Checkmark the time extraction and use the pattern as follows: *_*_*_*_*_*${startDate}*_*
6. In the parameter tab, click to add the sample points with latitude and longitude text file coordinates.

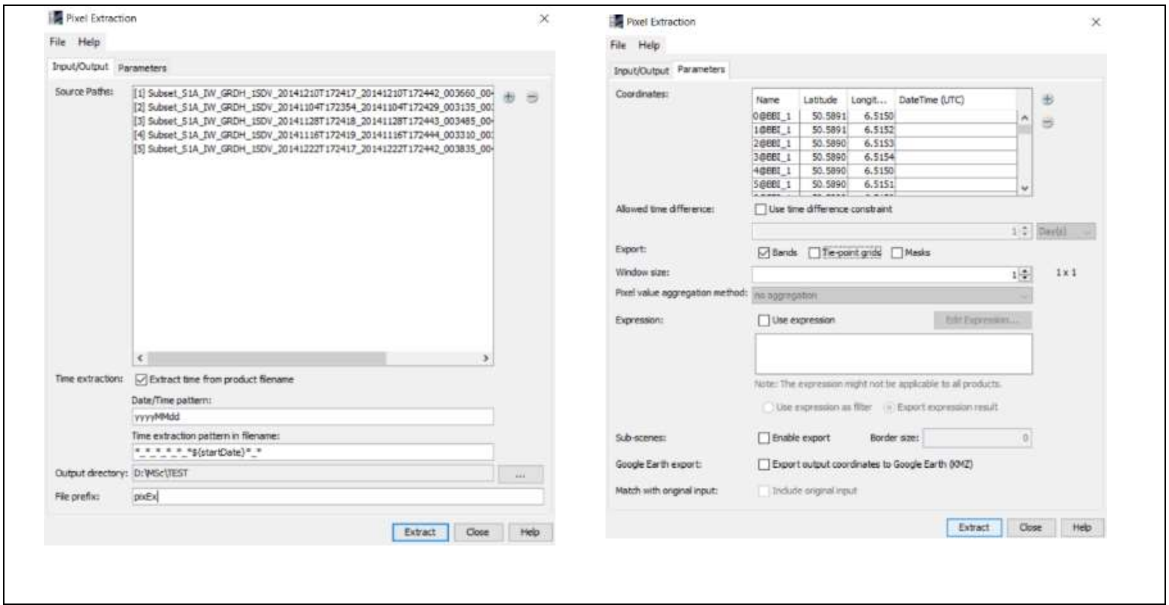

Appendix E. Checking the assumptions for t-test between infected and healthy samples

1. Test of equal variance assumption between infected and healthy sample spruce trees

F test to compare two variances
data: MyData1$VH_dB by MyData1$Infestations
F = 0.92835, num df = 2341, denom df = 2659, p-value = 0.06401
alternative hypothesis: true ratio of variances is not equal to 1
95 percent confidence interval:
0.8582843 1.0043408
sample estimates:
ratio of variances
0.9283525

The test fails to reject H0: there is no difference of variance between healthy and infected samples at the 0.05 threshold level since the p-value is 0.06 or greater than the threshold level.

2. Test of normality assumption using normal QQ plots for infected and healthy sample spruce trees

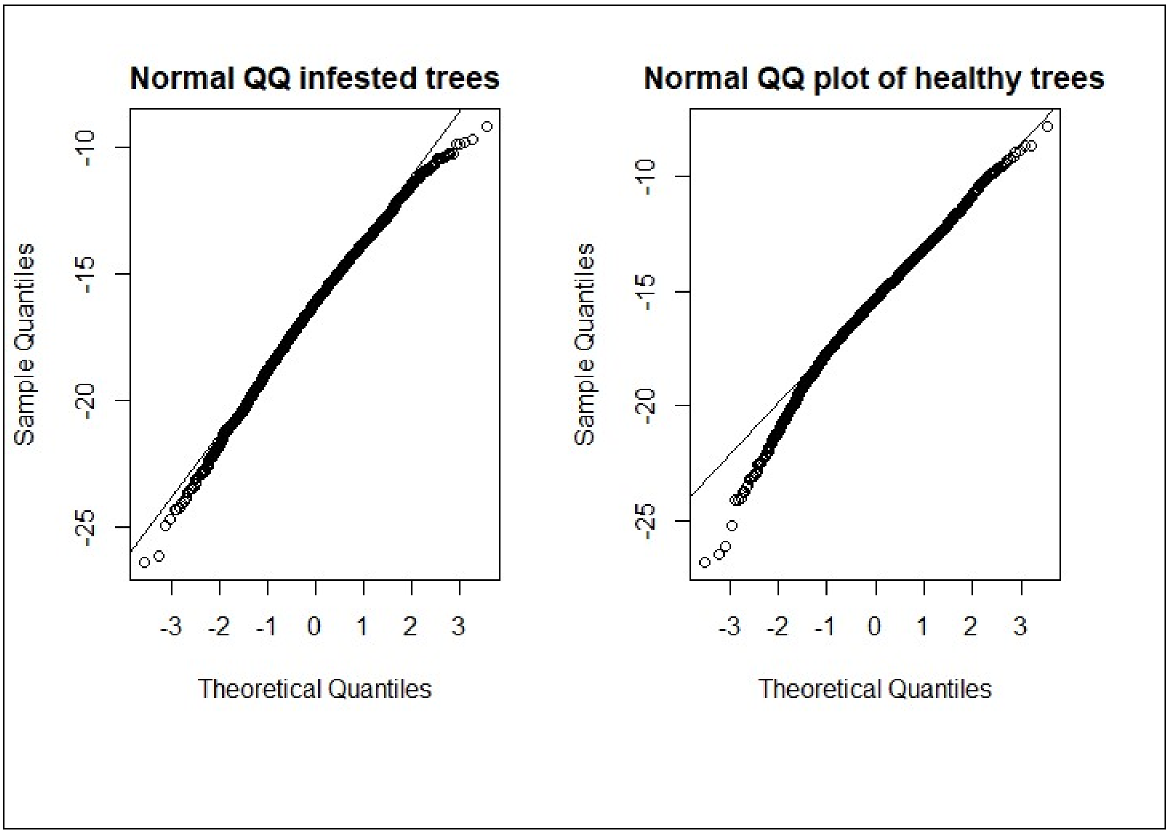

Although there are not many outliers but the majority of the data fall along the line which is safe to assume that data follows normal distributions.

Appendix F. A comparison of different speckle filters influence over the distribution of backscatter values between the healthy and bark beetles infected spruce trees.

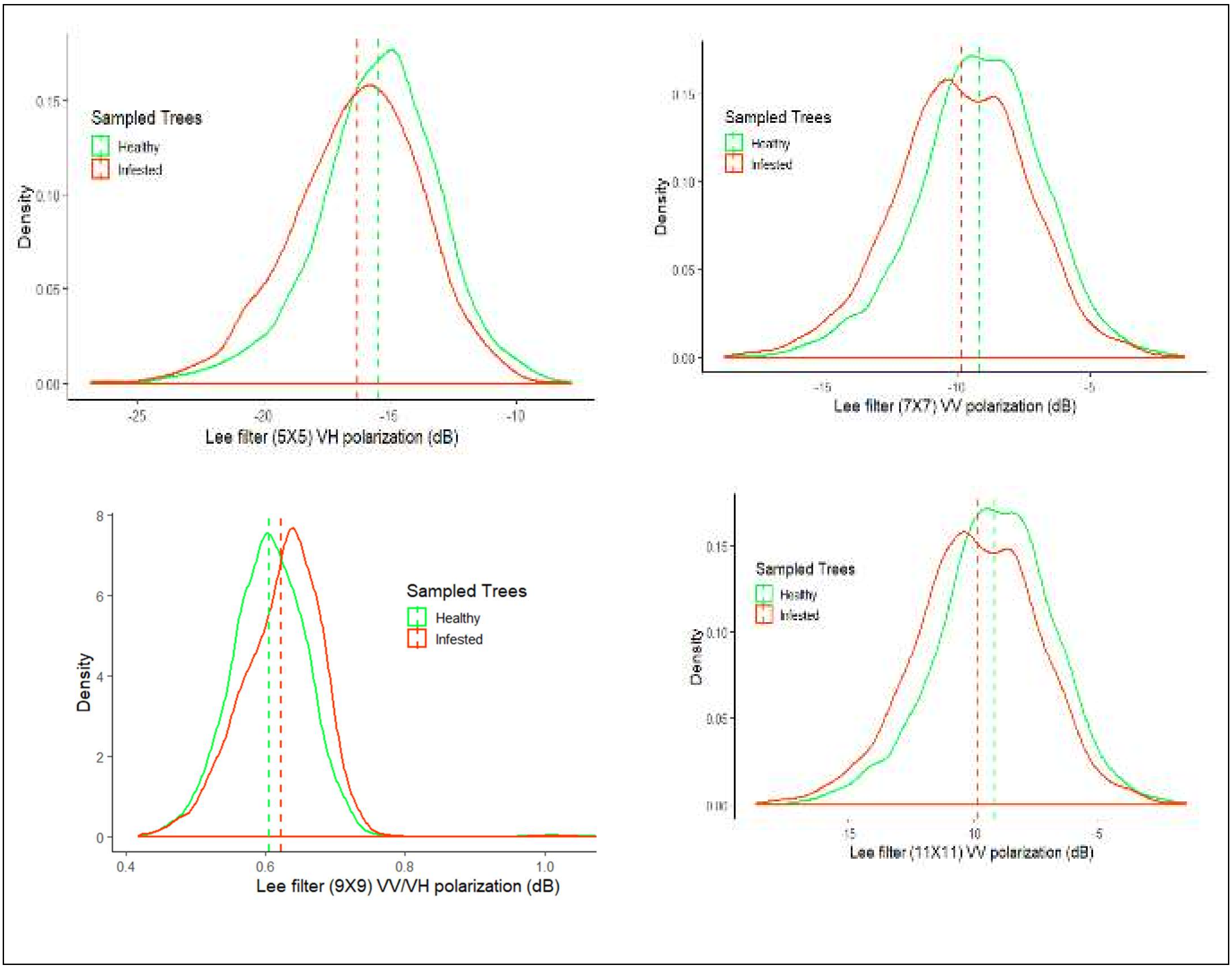

Appendix G. Google Eath Engine Java Scripts to extract SAR backscatter values to validate the bark beetle infestation moment.

```
//Coordinate of pixel obtained from GE for time profiling
var eifel = ee.Geometry.Point([7.2711074621, 50.5290127200]);

var yearly = ee.ImageCollection('COPERNICUS/S1_GRD')
    .filter(ee.Filter.eq('instrumentMode', 'IW'))
    .filter(ee.Filter.listContains('transmitterReceiverPolarisation', 'VH'))
    .filter(ee.Filter.eq('orbitProperties_pass', 'ASCENDING'))
    .filterBounds(eifel)
    .filterMetadata("platform_number","equals","A");

//Print the first image
print(yearly.first())

// Create a time series chart of the reference area
var chart = ui.Chart.image.seriesByRegion(
    yearly, eifel, ee.Reducer.mean(), 'VH', 10, 'system:time_start', 'Name')
        .setChartType('ScatterChart')
        .setOptions({
          title: 'Infestation Outside Study Area',
          vAxis: {title: 'VH'},
          lineWidth: 1,
          pointSize: 3,
          series: {
            //0: {color: 'green'}, // healthy
            //1: {color: 'red'} // infested
}});
print(chart, 'Rhienbroh Area');
```

Appendix H. R scripts for SAR backscatter analysis

```
knitr::opts_chunk$set(echo = T, message=FALSE, warning = F) # Message is set to `FALSE` to suppress the
 message being displayed in the output report

library(readxl)     # R package to read the excel data output from the SNAP
library(ggplot2)    # R package to make the graphs
library(scales)     # R package to prepare different measurement scales of the data for ggplot
library(lubridate)  # R package to handle date and time
library(tidyverse)  # for data munging
library(captioner)  # Label the figures and tables
library(knitr)      # Kniting Markdown documents

#read data sentinel 1 SAR pixel information of the sample
MyData1 <- read_excel("data/Backscatters1.xlsx")

#check the preview of fist 6 rows of data tables
head(MyData1)

# attaching data to r environment so that variable store in the columns of data frame can be accessed
attach(MyData1)

hist(Gamma0_VV, freq = F, density = 20)
lines(density(Gamma0_VV))

hist(Gamma0_VV_dB, freq = F, density = 20)
lines(density(Gamma0_VV_dB))

par(mfrow = c(1,2))

hist(Gamma0_VH, freq = F, density = 20)
lines(density(Gamma0_VH))

hist(Gamma0_VH_dB, freq = F, density = 20)
lines(density(Gamma0_VH_dB))
```

.

```
# Gamma0_VV_dB
n <- MyData1 %>%
  ggplot( aes(x=Gamma0_VV_dB, fill=Infestations, stat(density))) +
  geom_histogram( color="#e9ecef", alpha=0.75, position = 'identity') +
  scale_fill_manual(values=c("#00ff40", "#ff4000")) +
  xlim(-17, -1) +
  #theme_ipsum() +
  labs(fill="")+
  theme(legend.position = c(0.2, 0.7))
n
```

```
# Gamma0_VH_dB
n <- MyData1 %>%
  ggplot( aes(x=Gamma0_VH_dB, fill=Infestations, stat(density))) +
  geom_histogram( color="#e9ecef", alpha=0.75, position = 'identity') +
  scale_fill_manual(values=c("#00ff40", "#ff4000")) +
  xlim(-21, -7) +
  #theme_ipsum() +
  labs(fill="")+
  theme(legend.position = c(0.2, 0.7))
n

# compare basckatters of infestations and healthy trees
#boxplot(Gamma0_VH_dB~Infestations)
# Change box plot line colors by groups
p<-ggplot(MyData1, aes(x="", y = Gamma0_VH_dB, color=Infestations) ) +
  geom_boxplot(outlier.shape = 23, outlier.color = "black") +
  scale_color_manual(values=c("#00ff40", "#ff4000")) +
#theme_ipsum() +
  labs(fill="", color = "Spruce tree class") +
  theme(legend.position = c(0.9, 0.2))
```

```r
#p <- p + coord_fixed(ratio = 0.06)
p
```

.

```r
## compare difference of meam to infestation

#signal <- cbind(Gamma0_VH, Gamma0_VV,Gamma0_VH_dB,Gamma0_VV_dB,Gamma0_VH_CR_VV,Gamma0_VHdB_CR_VVdB,Gamma0_VH_diff_VV)

signal <- cbind(Gamma0_VH, Gamma0_VV,Gamma0_VH_dB,Gamma0_VV_dB )
bc1 <- manova(signal~Infestations)
summary(bc1)

##                Df Pillai approx F num Df den Df    Pr(>F)
## Infestations    1 0.2562    430.3      4   4997 < 2.2e-16 ***
## Residuals    5000
## ---
## Signif. codes:  0 '***' 0.001 '**' 0.01 '*' 0.05 '.' 0.1 ' ' 1

sar_ht <- read_excel("data/sar_ht.xlsx",
    col_types = c("text", "date", "numeric",
        "numeric"))
sar_it <- read_excel("data/sar_it.xlsx",
    col_types = c("text", "date", "numeric",
        "numeric"))

head(sar_ht)

# Healthy trees
ht_VH <- sar_ht %>%
  select(Name, Date, Sigma0_VH_db ) %>%
  spread(Name, Sigma0_VH_db)
ht_VV <- sar_ht %>%
  select(Name, Date, Sigma0_VV_db ) %>%
  spread(Name, Sigma0_VV_db)

# infected trees
it_VH <- sar_it %>%
  select(Name, Date, Sigma0_VH_db ) %>%
  spread(Name, Sigma0_VH_db)
it_VV <- sar_it %>%
  select(Name, Date, Sigma0_VV_db ) %>%
  spread(Name, Sigma0_VV_db)

#Join by Date column for each VV and VH dB Polarization
df_VH <- full_join(ht_VH, it_VH, by="Date")
df_VV <- full_join(ht_VV, it_VV, by="Date")

VH_data <- df_VH %>%
  select(Date, Healthy30, Infected42) %>% # Subsitude any sample of choice HERE
  gather(key = "status", value = "value", -Date)

g <- ggplot(data = VH_data,
            aes(x = as.Date(Date), y = value,color = status)) +
  scale_color_manual(values = c("#00ff40", "#ff4000")) +
  #geom_line() +
  geom_smooth(span=0.08, se=F) +
  scale_x_date(breaks = date_breaks("1 years"), date_labels = "%Y")
g <- g + coord_fixed(ratio = 150) +
  theme(axis.text = element_text(face = "bold", size = rel(.8))) +
  labs(title = "SAR temporal profile of healthy and bark beetle infected tree",
       x = "Year",
       y = "SAR VH backscatter (dB)",
       color = "Tree status")
scale_y_continuous(labels = function(a) paste0(a/1,"dB"))
```

Appendix I. Temporal profiles of healthy and infected centre points of their sample polygon